เอกสารแนบหมายเลข 1



**Final Report**

# Renewable Bio-oxygenated Fuel Particle Emission Trapping and Oxidation Behaviors inside Ceramic Micro-porous of Diesel Particulate Filters

**By Asst.Prof.Dr.Preechar Karin**

July / 2559

Contract No. TRG5780301

**Final Report**

# Renewable Bio-oxygenated Fuel Particle Emission Trapping and Oxidation Behaviors inside Ceramic Micro-porous of Diesel Particulate Filters

**Asst.Prof.Dr.Preechar Karin**

**King Mongkut's Institute of Technology Ladkrabang**

**This project granted by the Thailand Research Fund**

## Abstract

**Project Code : TRG5780301**

**Project Title : Renewable Bio-oxygenated Fuel Particle Emission Trapping and Oxidation Behaviors inside Ceramic Micro-porous of Diesel Particulate Filters**

**Investigator : Asst.Prof.Dr.Preechar Karin**
**King Mongkut's Institute of Technology Ladkrabang**

**E-mail Address : kkpreech@staff.kmitl.ac.th, preechar.ka@kmitl.ac.th**

**Project Period : August 1, 2014 – July 31, 2016**

The impact of small compression ignition (CI) engine operation conditions and fuel properties on diesel and biodiesel particulate matters (PMs) quantity using opacity smoke meter is investigated. The biodiesel engine's PMs are around a half of diesel engine PMs under the same engine operation conditions. Morphology of both engine's PMs are also studied using a Scanning Electron Microscopy (SEM), Transmission Electron Microscopy (TEM) and image processing method. The average primary nanoparticle sizes of diesel and biodiesel engine's PMs are approximately 34 nm and 32 nm, respectively. The result shows that engine operation condition and fuel property are strongly impact on the quantity and size distribution of primary nanoparticles emission. PM oxidation kinetics on conventional cordierite Diesel Particulate Filters (DPFs) powders by Thermo-gravimetric analysis (TGA) is also successfully studied. The calculated apparent activation energies of biodiesel engine's PM oxidation on conventional cordierite DPFs powders are lower than that of diesel engine's PM and carbon black because of unburned oxygenated molecule. The calculated apparent activation energy of biodiesel engine's PM and diesel engine's PM oxidize on conventional cordierite DPFs powders with pure air are in the range of 109-131 kJ/mole and 117-130 kJ/mole, respectively. It might be expected that smaller primary nanoparticle size of biodiesel engine's PMs and bio-oxygenate unburned hydrocarbon can promote more PM oxidation rate during vehicle's DPF regeneration process.

**Keywords :** Engine, Particulate Matter, Particulate Filter, Biodiesel, Oxidation Kinetics

## Executive summary

Among conventional internal combustion engines (ICEs), direct injection diesel engine or compression-ignition (CI) engines have the highest thermal efficiency for a given output power. However, diesel engines are an important source of particulate matters (PMs). PMs must be removed from the exhaust gas emitted from engines to protect the human health. The objectives of the present research are to investigate the impact of biodiesel fuel on morphology and oxidation kinetics of engine's PMs on conventional Diesel Particulate Filter (DPF) powders by using TEM and TGA, respectively. Primary particle size distribution and oxidation apparent activation energies would be calculated by using TEM image processing method and Arrhenius plots of PM oxidation kinetics for better understanding. In addition, particulates trapping and oxidation behaviors in a DPF surface are also successfully investigated.

Figure 1 shows quantity of diesel engine's PMs and biodiesel engine's PMs using opacity smoke meter in the condition 20, 40, 60 and 80% of engine load, 1600, 1800, 2000, 2200 and 2400 rpm of engine speed. The quantities of PMs emitted from biodiesel engine are approximately half of diesel engine because of bio-oxygenate fuel.

Figure 2 shows SEM and TEM images of a biodiesel engine's PM sample, captured by paper filter using smoke meter. It was clearly observed that PM10 is a group of agglomerated PMs. The agglomerate ultrafine particle and primary nanoparticle size were micron and submicron scale, respectively. The average agglomerate ultrafine particle sizes of both diesel and biodiesel engine's PMs are approximately 100-500 nm. Engine's agglomerate ultrafine particles consist of several uniform primary nanoparticles. Most of engine's primary nanoparticle diameter is smaller than 60 nm.

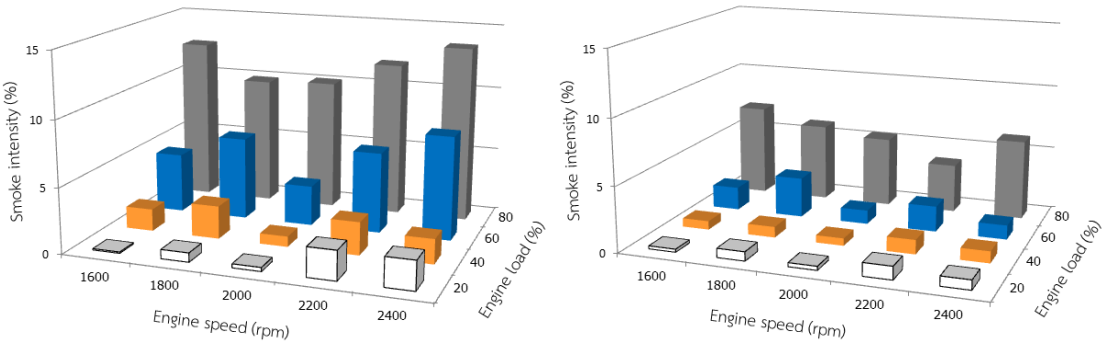


Diesel Engine's PMs  Biodiesel Engine's PMs

Figure 1 Quantity of (left) diesel engine's PMs and (right) biodiesel engine's PMs using opacity smoke meter in each engine load and engine speed operation condition.

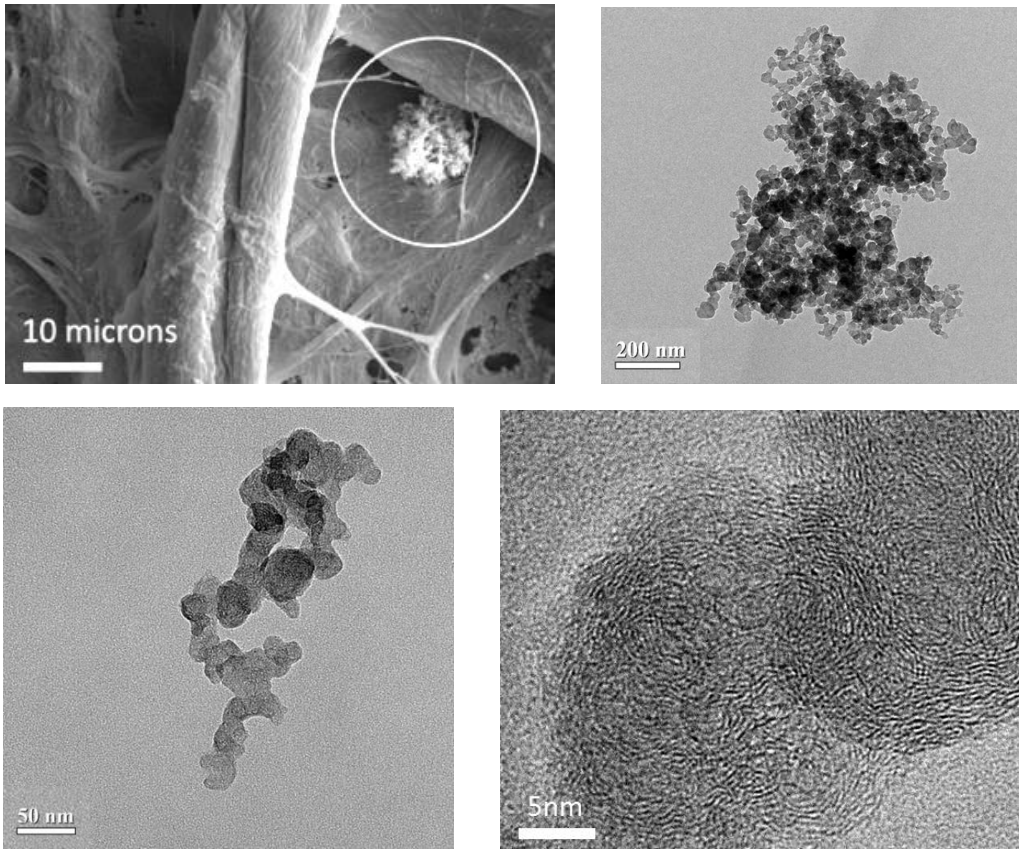


Figure 2 SEM and TEM images of biodiesel engine's PM10, morphology of agglomerated ultrafine particles and nanostructure of nanoparticles.

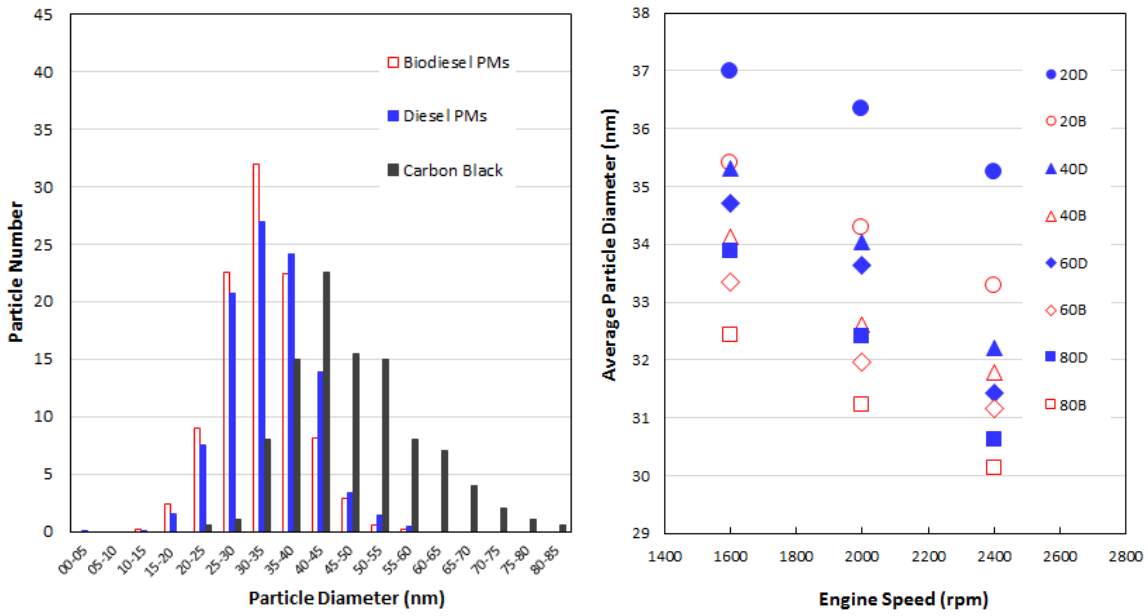


Figure 3 Average size distribution of diesel engine's nanoparticles and biodiesel engine's nanoparticles under 20, 40, 60 and 80% of engine load and 1600, 2000 and 2400 rpm of engine speed using TEM image processing method.

Figure 3 shows the average diameter size of diesel engine's nanoparticles versus biodiesel engine's nanoparticles in 20, 40, 60 and 80% of engine load and 1600, 2000 and 2400 rpm of engine speed. The average diameter of biodiesel engine's PMs are significantly smaller than that of diesel engine's PMs because of bio-oxygenate fuel. The average diameter of primary nanoparticles emitted from engine all operation conditions and carbon black are in the range of 10-60 nm and 20-90 nm, respectively. The average single particle sizes of carbon black, diesel and biodiesel engine's PMs are approximately 48, 34 and 32 nm, respectively.

Figure 4 shows mass conversions of carbon black, diesel engine's PMs and biodiesel engine's PMs oxidation with pure air on DPF powders using TGA isothermal method. Absolutely, engine's PMs oxidation rate is higher than carbon black. It was clearly seen that biodiesel engine's PMs were oxidized faster than diesel engine's PMs. The Apparent activation energies of engine's PMs oxidation on conventional cordierite DPF powders with pure air are in the range of 109-131 kJ/mole. The lowest apparent activation energy occurred in 20-40% of mass burned fraction. Whereas, the highest apparent activation energies of 60-80% of biodiesel and diesel engine's PMs.

The pressure drop between the inlet and outlet of the DPF wall during diesel PMs trapping was approximately 2 times higher than that of biodiesel PMs. This could be explained that more soot particle was remained in diesel combustion than those of biodiesel. Because it contains oxygen molecule, biodiesel is readily oxidized with available oxygen in the flame zone. It's also clearly observed that the oxidation rate of biodiesel PMs on the DPF wall surface was higher than that of diesel PMs for all of conditions.

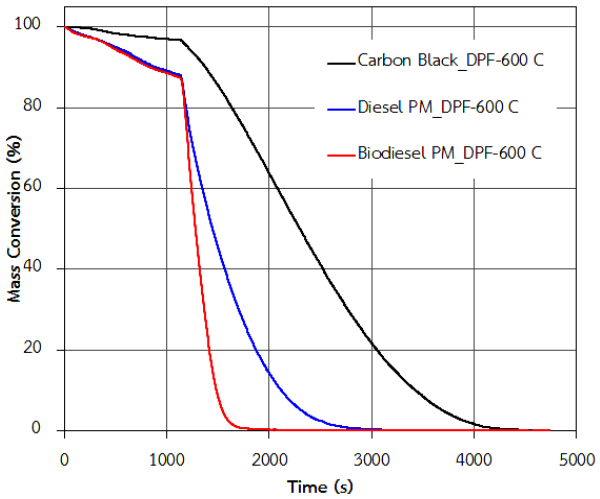


| | Apparent Activation Energy *Ea* (kJ/mole) |
|---|---|
| **PMs Oxidize with DPF Powder** | |
| **PMs Burned Fraction** | |
| Biodiesel Engine's PMs | 121±11 |
| Biodiesel 20-40% burned | 109 |
| Biodiesel 40-60% burned | 121 |
| Biodiesel 60-80% burned | 131 |
| Diesel Engine's PMs | 124±7 |
| Diesel 20-40% burned | 117 |
| Diesel 40-60% burned | 124 |
| Diesel 60-80% burned | 130 |

Figure 4 Oxidation kinetics of carbon black, diesel engine's PMs and biodiesel engine's PMs on conventional cordierite DPF powders using TGA isothermal method with pure air.

## Objectives

- Physical and chemical characterization of fossil and renewable bio-oxygenated fuels particulate matters (PMs) emitted from a conventional diesel engine.
- Characterization of fossil and renewable bio-oxygenated fuels PMs trapping and oxidation kinetics in a conventional Diesel Particulate Filters (DPFs).

## Research methodology

- Physical and chemical characterization of fossil and renewable bio-oxygenated fuels particulate matters (PMs) emitted from a conventional diesel engine by Optical Microscopy, Scanning Electron Microscopy (SEM), Transmission Electron Microscopy (TEM), Energy Dispersive Spectroscopy (EDS), Thermo-gravimetric Analysis (TGA) and Carbon-hydrogen-nitrogen Thermal Analysis (CHN), Laser Diffraction Technique, etc.
    - It is clearly observed that the primary particle size and quantity of renewable bio-oxygenated fuel are smaller than that of diesel because the oxygen content in biodiesel might have effects on particle combustion. Mechanisms of soot formation and combustion inside engine should be explained for the different size distribution of each renewable bio-oxygenated fuel and fossil fuel.
- Characterization of fossil and renewable bio-oxygenated fuels PMs trapping and oxidation kinetics in a conventional Diesel Particulate Filters (DPFs) by a DPF analyzer.
    - PM trapping and oxidation behaviors of renewable bio-oxygenated fuel would be investigated to compare with that of fossil fuel. Pressure drop and temperature between inlet and outlet of DPF must be monitored during trapping and oxidation processes. Finally, mechanisms of PM trapping and oxidation inside conventional DPF also should be proposed in this research.

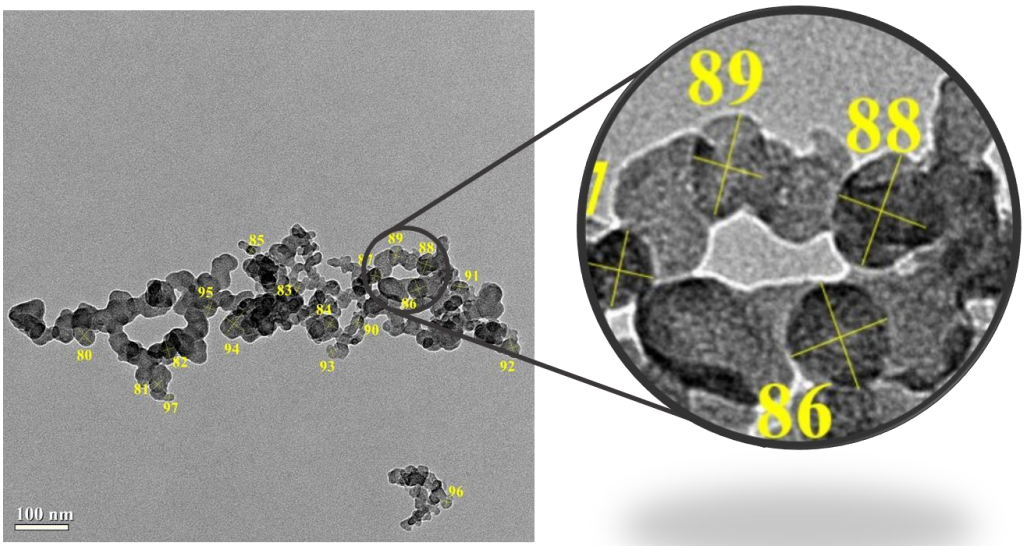


Figure 5 TEM image processing for primary particle of PM analysis.

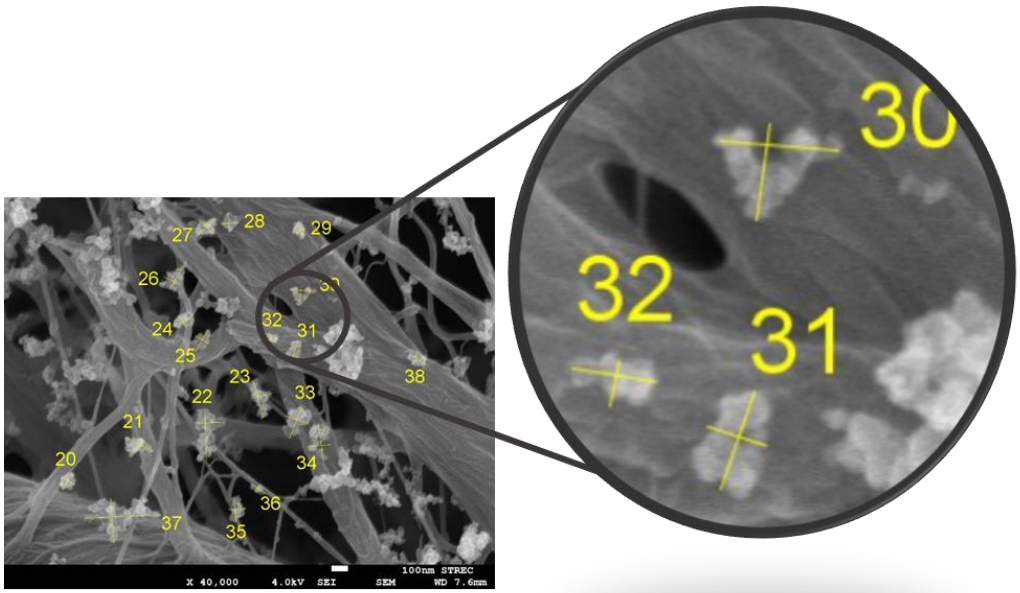


Figure 6 SEM image processing for agllomerate particle of PM analysis.

**Research Result and Discussion**

## INTRODUCTION

Particulate matter (PMs) must be removed from the exhaust gas emitted from internal combustion engines (ICEs) to protect the human health. Physical and chemical PMs characterization methods for both of spark ignition (SI) and compression ignition (CI) engines under various vehicle certification cycles and real-world driving conditions are reviewed (Choi *et al*., 2014). Physical properties of engine's PMs have been reported by several researchers. The formation of PMs is through to take place via a number of elemental steps: pyrolysis, nucleation, surface growth and coagulation, aggregation and oxidation. These processes take place on different time scales, ranging from a few microseconds to some milliseconds (Neeft *et al*., 1996).

Surface growth is the process in which the precursor molecules grow from nanoparticles. Simultaneously, another process takes place: coagulation. Small particulates collide and coalesce, forming larger spherical particles. Aggregation or chain-forming coagulation accounts for the formation of the well-known "fractal" structure of soot (Eastwood, 2008). The carbon atoms are bonded together in hexagonal face-centered arrays in planes commonly referred to as platelets. Platelets are arranged in layers to form crystallites (Smith, 1981). Diesel engine's PMs consists of two particles: i) fractal-like agglomerates of primary particles, consisting of carbon and traces of metallic ash, and coated with condensed heavier and organic compounds and sulfate, and ii) nucleation particles composed of condensed HCs and sulfate (Maricq, 2007).

Scanning Electron Microscopic (SEM) and Transmission Electron Microscope (TEM) observation of particulate matters have been conducted by several researchers. A primary processed soot particle has two distinct parts: an inner core and an outer shell (Ishiguro, *et al*., 1997). Generally, a primary particle has only one core with concentric fringe pattern which is hard to be distinguished as inner core and outer shell of internal combustion engine PMs. Some primary particles were found to have a hollow interior and the outer shell exhibiting evidence of graphitization, with a higher crystalline than the non-hollowed particles (Vander Wal, *et al*., 2007). Size distributions of diesel engine's PMs have been reported by several researchers. Most of the particle mass exists in the accumulation mode in the diameter range of few hundred nanometers. Size definitions for atmospheric particles are PM10, diameter ($D$) < 10 μm; fine particles, $D$ < 2.5 μm; ultrafine particles, $D$ < 0.10 μm; and nanoparticles, $D$ <

0.05 μm or 50 nm (Kittelson, 1998). The particles in the size range from 20 to 200 nm are very sensitive to sudden changes of the engine operation conditions (Soylu, 2014).

The oxidation behavior of PMs has been investigated using Thermo-gravimetric Analysis (TGA) and Temperature Program Oxidation (TPO) to evaluate reaction activity. The fit curve results of reaction order for both oxygen and processed soot, and the activation energies, were defined and reported. The reaction order of soot and pure solid carbon particle are in the range of 0.5-1 due to complex structure of agglomerate particles. The activation energy ($E_a$) of carbon oxidation is around 150-170 kJ/mole. However, the reaction order of the engine PMs has broader range than the processed soot due to the various crystalline structure and impurity, and also changes with soot conversion (Neeft *et al*., 1997; Darcy *et al*., 2007; Yezerets *et al.*, 2005; Fino *et al*., 2008, Lee *at al.*, 2013; Choi *et al.*, 2015; Karin *et al*, 2015).

Diesel engine after-treatment technology that substantially reduces particle emissions is Diesel Particulate Filters (DPFs). The DPF plays an important role in PM trapping and oxidation. These processes involve the most complex behavior of PMs and chemical reaction phenomena. Mechanisms of engine's PM trapping and oxidation on DPF wall surface were successfully clarified via real-time macro-microscopic visualization method (Hanamura *et al*., 2009; Karin *et al*., 2010; Oki *et al*., 2011).

The effects of engine technologies, fuels, and engine lubricant oils on PM morphology and chemical compositions are also discussed (Myung *et al*., 2014). Biodiesel fuel engine's PMs were investigated and compared with the conventional diesel fuel. PM diameter size and quantity of biodiesel engine are smaller than that of diesel engine. It might be the effect of oxygenated fuel promotes more completely combustion and makes smaller size exiting (Karin *et al*., 2013). In the case of biodiesel fuel engine, especially, measured particle parameters such as single particle size and the radius of gyration were decreased compared to those of conventional diesel fuel (Lee *et al*., 2013).

The objectives of the present research are to investigate the impact of biodiesel fuel on morphology and oxidation kinetics of engine's PMs on conventional DPF powders by using TEM and TGA, respectively. PM size distribution and oxidation apparent activation energies would be calculated by using TEM image processing method and Arrhenius plots of PM oxidation kinetics for better understanding and future design of DPF configuration for biodiesel blends diesel engine application.

## METHODOLOGY

### Particulate Matters Physical Characteristics

Table 1 Physical and chemical fuels properties

| Fuel Properties | Biodiesel | Diesel |
|---|---|---|
| Cetane Number | 70 | 55 |
| Heating Value (kJ/kg) | 39,550 | 46,800 |
| Density (kg/$m^3$) | 847.73 | 844.78 |
| Viscosity (cSt) | 4.5 | 3.0 |
| Flash point (°C) | 70 | 64 |
| Carbon Fraction | 78 | 82 |
| Chemical Formula | $C_{15.3}H_{29.5}O_{1.7}$ | $C_{16.2}H_{32.0}$ |

Table 2 Engine operation conditions

| Engine load (%) | 0 | 20 | 40 | 60 | 80 | 100 |
|---|---|---|---|---|---|---|
| Torque (Nm) | - | 9.5 | 19 | 28.5 | 38 | 47.5 |

A conventional diesel fuel (B5) and biodiesel fuel derived from palm-olein (B100: TIS 2313-2549) were used in this research, as shown in Table 1. The engine has displacement of 638 $cm^3$ and a rated output of 8.8 kW. The engine is a single cylinder, four strokes and direct injection. The fuel injection pressure was approximately 19.6 MPa. The engine was operated by constant speed of 1600, 1800, 2000, 2200 and 2400 rpm and 0, 20, 40, 60 and 80% load on the Eddy current engine dynamometer (Tokyo plant ED-60-LC), as shown in Table 2.

Engine's PMs quantity were measured using opacity diesel smoke meter (OKUDA DSM-240), which optically evaluate soot collected on paper filters. The measuring method is light reflection method in the range of 0-100%, ±3% of measuring accuracy. In addition, engine exhaust's PM samples were collected using in-house metal-net engine particle emission collector. The particle emission collector is located on exhaust manifoild. Optical microscopy (OLYMPUS BX51), scanning electron microscopy (SEM: EVO MA10), transmission electron microscopy (TEM: JEOL JEM-2010) and ImageJ softwear (http://imagej.net) image processing method were used to characterize diesel and biodiesel engine's PM morphology, nanostructure and primary particle size distribution.

**Particulate Matters Chemical Characteristics**

Engine's PM samples were collected at 2400 rpm of constant engine speed and 80% of engine load using in-house metal net engine particle emission collector. PM oxidation kinetics were investigated by using thermo-gravimetric analysis (TGA: METTLER TOLEDO TGA/SDTA851e) method with 0.1 mg sensitivity, 0.1% accuracy of balance mass and 2 °C of temperature error. The conventional cordierite diesel particulate filter (DPF) was milled to be powders. DPF powders were mixed with carbon black (grade: N330), diesel PMs and biodiesel PMs using manual mortar grinding machine. Figure 1 shows conventional DPF upstream surface EDS analysis. It was clearly observed cordierite DPF composition, such as Si, Al, Mg, Fe, O, C, Au, Ce, Fe etc. Figures 2 show SEM images of (a) DPF upstream surface, (b) DPF wall cross-sectional area and (c) DPF downstream surface before mixed with carbon black and PMs using manual mortar grinding machine.

Isothermal method was used to investigate oxidation kinetics of carbon black, diesel PMs and biodiesel PMs on DPF powders. Each mixed sample was tested at three different constant temperature including 500, 550 and 600 °C. Nitrogen was used to heat up the sample to desired temperature then pure air is introduced for soot oxidation for one hour. Chemical kinetics of PMs oxidation is studied by using mass conversion behavior from TGA. The chemical reaction rate in Eq.1 can be calculated from the TGA mass conversion curve based on the chemical kinetic in Eq.2. Where ***C*** is PM mass, ***t*** is time, ***n***, ***m*** are the reaction order of PM and oxygen, respectively. The reaction order **n** is assumed to be 2/3 (0.67) as shrinking core model because PM is also assumed to be spherical shape for simplicity. In order to calculate the apparent activation energy (***Ea***) of PM oxidation, the chemical reaction rate constant ***k*** at each temperature in Eq.2 is expressed by Eq.3. Where ***A*** is the frequency factor, ***Ea*** is the activation energy, ***R*** is the gas constant. Finally, the apparent activation energy can be calculated by Eq.4 using the Arrhenius plot.

$$C + O_2 \rightarrow CO_2 \tag{1}$$

$$-\frac{d[C]}{dt} = k[C]^n[O_2]^m \tag{2}$$

$$k = Ae^{-\frac{E_a}{RT}} \tag{3}$$

$$\ln\left[\frac{-1}{[C]^n}\frac{d[C]}{dt}\right] = -\frac{E_a}{RT} + (\ln A + m\ln[O_2]) \tag{4}$$

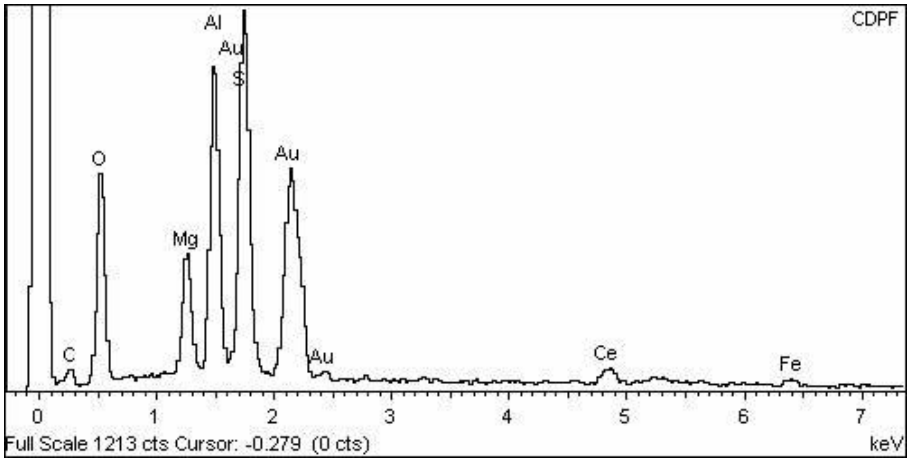


Figure 1 EDS analysis of a conventional cordierite DPF microstructure upstream surface before particulate matters mixing and TGA analysis.

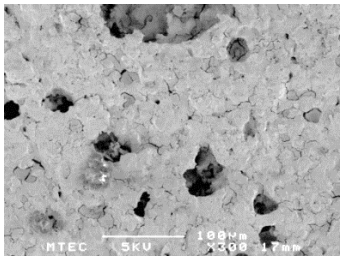

(a) SEM image of DPF upstream surface

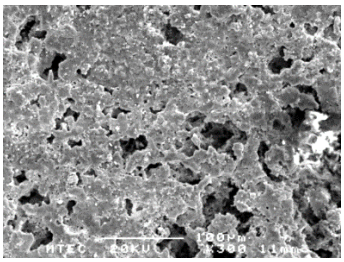

(b) SEM image of DPF wall cross-sectional area

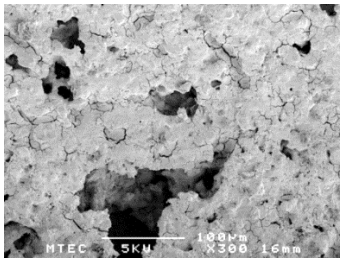

(c) SEM image of DPF downstream surface

Figure 2 SEM images of a conventional cordierite DPF microstructure of (a) DPF upstream surface, (b) DPF wall cross-sectional area and (c) DPF downstream surface, before mixed with carbon black and PMs for TGA analysis.

## RESULTS

### Particulate Matters Quantity and Morphology

Figures 3 show SEM images of biodiesel engine's PM in the condition 80% of engine load and 2400 rpm of engine speed, captured by paper filter using smoke meter. Trapped PM10 were clearly observed as shown in white circle. It was clearly observed that PM10 is a group of agglomerated PMs. Morphology of biodiesel's engine PM10 are not significant different from that of diesel's engine.

Figures 4 show quantity of (a) diesel engine's PMs and (b) biodiesel engine's PMs using opacity smoke meter in the condition 20, 40, 60 and 80% of engine load, 1600, 1800, 2000, 2200 and 2400 rpm of engine speed. The result shows that engine's PMs increased with engine load. It might be expected that increasing load or amount of fuel injection resulting in increasing of PMs. Large amount of engine's PMs was clearly observed in both low and high engine speed whereas small amount of engine's PMs in the medium engine speed which is the condition of lowest engine energy consumption. Absolutely, the quantities of PMs emitted from biodiesel engine are approximately half of diesel engine because of bio-oxygenate fuel.

The agglomerate ultrafine particle and primary nanoparticle size were micron and submicron scale, respectively. Engine's agglomerate ultrafine particles consist of several uniform primary nanoparticles. Most of engine's primary nanoparticle diameter is smaller than 60 nm. The average agglomerate ultrafine particle sizes of both diesel and biodiesel engine's PMs are approximately 100-500 nm. Figure 6 and 7 show TEM images of biodiesel and diesel engine's ultrafine PMs under the condition 80% of engine load, 2400 rpm of engine speed and carbon black ultrafine particles. The average agglomerated ultrafine particle's diameter of carbon black is significant larger than that of diesel and biodiesel engine PMs. Primary nanoparticles of both diesel and biodiesel engine's PMs were measured using image processing method.

One hundred primary nanoparticles of each case are successfully measured using the image processing software. Figures 8 and 9 show biodiesel and diesel engine's primary nanoparticle size distribution in the condition 20, 40, 60 and 80% of engine load and (a) 1600, (b) 2000 and (c) 2400 rpm of engine speed, respectively. The primary nanoparticle diameters are in the range of 10-60 nm. It was clearly observed much amount of particle diameters are in the range of 30-40 nm.

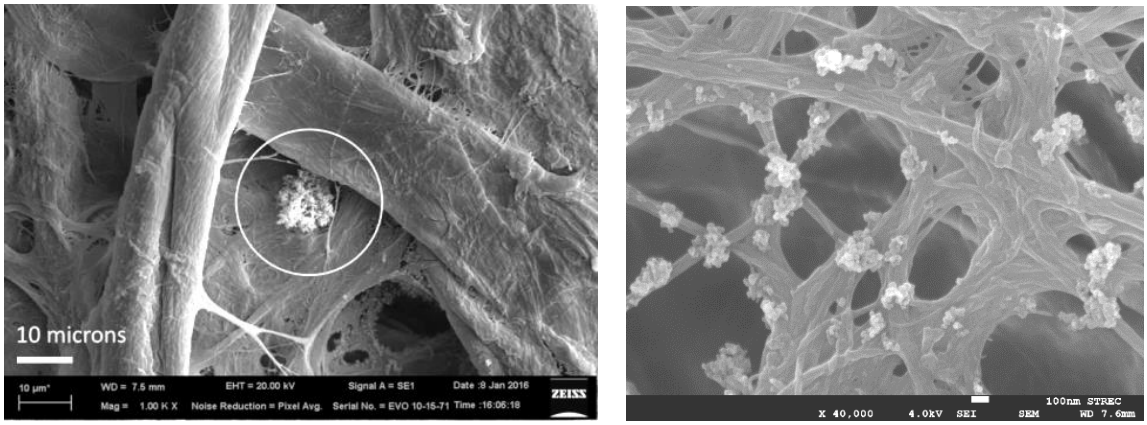


Figure 3 SEM image of biodiesel engine's PM10 in the condition 80% of engine load and 2400 rpm of engine speed, captured by glass fiber filters.

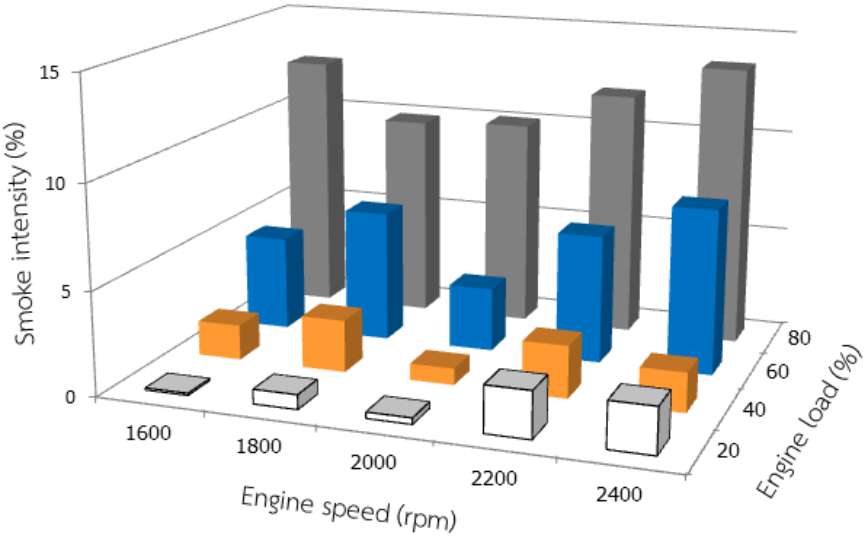


(a) Diesel Engine's Particulate Matters

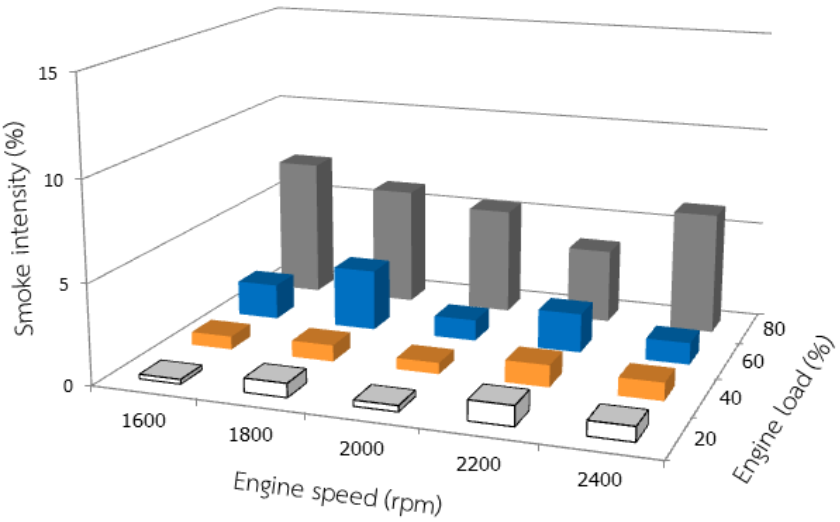


(b) Biodiesel Engine's Particulate Matters

Figure 4 Quantity of (a) diesel engine's PMs and (b) biodiesel engine's PMs using opacity smoke meter in each engine load and engine speed operation condition.

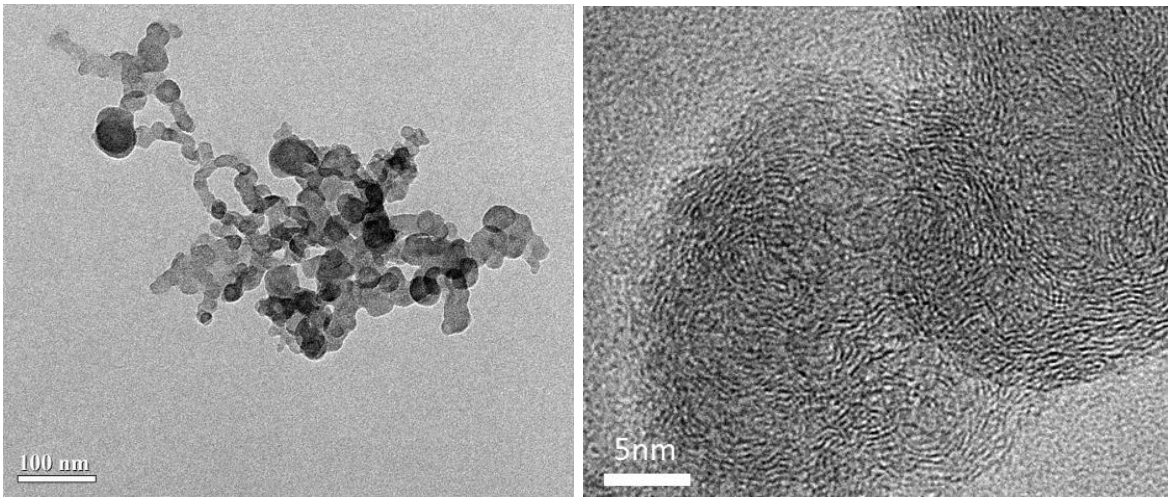


(a) Biodiesel Engine's Ultrafine Particle b) Biodiesel Engine's Nanoparticle

Figure 5 TEM images of biodiesel engine's (a) ultrafine particles and (b) nanoparticles in the operation condition 80% of engine load and 2400 rpm of engine speed.

Figure 10 shows the average diameter size of diesel engine's nanoparticles versus biodiesel engine's nanoparticles in 20, 40, 60 and 80% of engine load and 1600, 2000 and 2400 rpm of engine speed. Particle diameter size decreased when increasing engine speed for both of diesel and biodiesel's engine PMs. The exhaust gas temperature also gradually increased when increasing engine speed. It means PM oxidation rate inside combustion chamber increased when increasing engine speed (increasing temperature) due to lower heat loss on cylinder surface compare to lower engine speed. Similarly, particle diameter size decreased when increasing engine load for both of diesel and biodiesel's engine PMs. The exhaust gas temperature also gradually increased when increasing the engine load. It means PM oxidation rate inside combustion chamber increased when increasing engine load (increasing fuel injection quantity) resulting in higher combustion temperature compare to lower engine load.

Moreover, the average diameter of biodiesel engine's PMs are significantly smaller than that of diesel engine's PMs because of bio-oxygenate fule. The average diameter of primary nanoparticles emitted from engine all operation conditions and carbon black are in the range of 10-60 nm and 20-90 nm, respectively, as shown in Fig.11. The average single particle sizes of carbon black, diesel and biodiesel engine's PMs are approximately 48, 34 and 32 nm, respectively. In addition, the average agglomerate particle size are in the range of 150-200 nm for both diesel and biodiesel PMs. The average agglomerated particle size of biodiesel engine PM is also smaller than that of diesel engine PM, as shown in Fig.12-14.

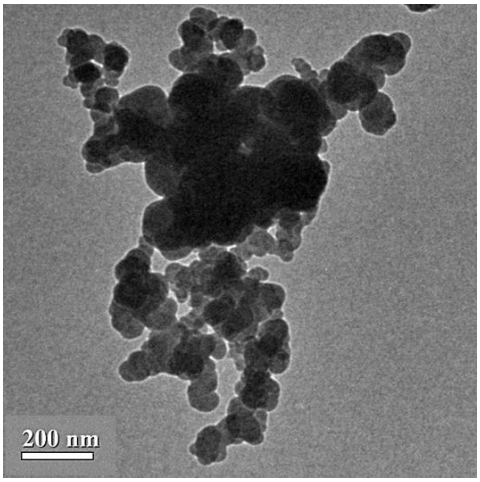


(a) Carbon Black Ultrafine Particle

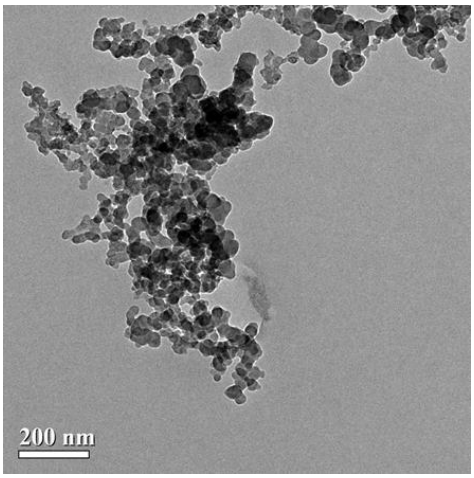


(b) Diesel Engine's Ultrafine Particle

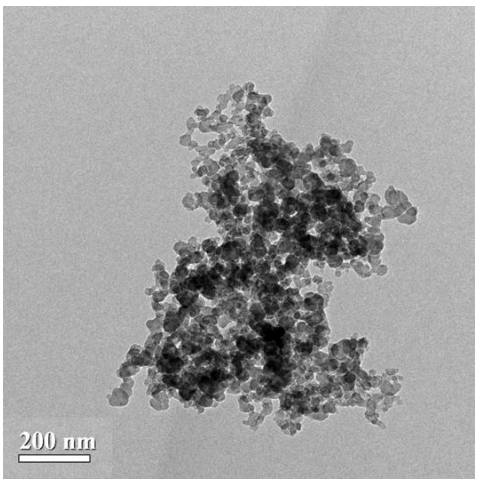


(c) Biodiesel Engine's Ultrafine Particle

Figure 6 TEM images of (a) carbon black, (b) diesel engine's ultrafine particles and (c) biodiesel engine's ultrafine particles in the operation condition 80% of engine load and 2400 rpm of engine speed.

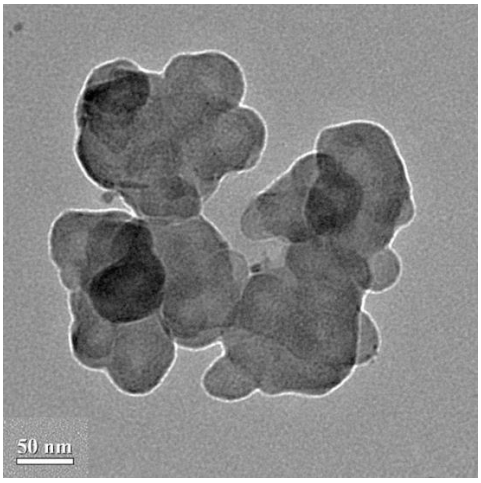


(a) Carbon Black Ultrafine Particle

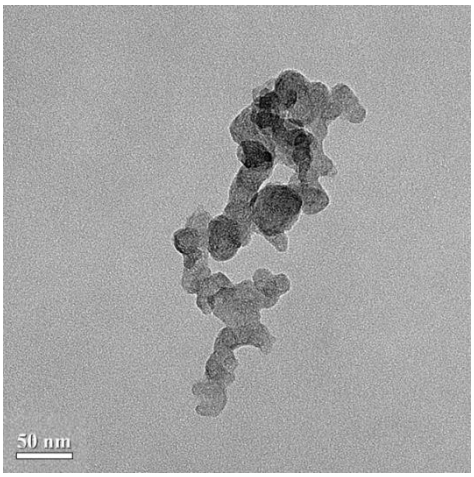


(b) Diesel Engine's Ultrafine Particle

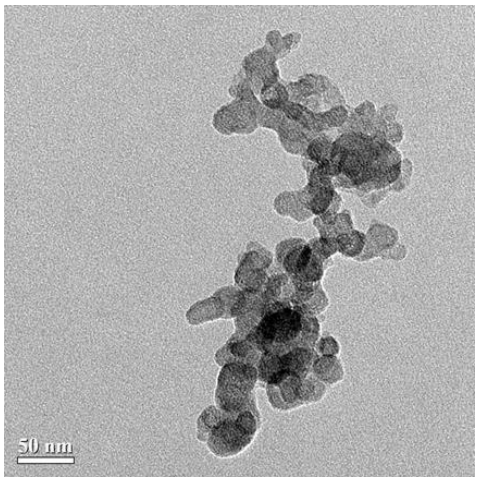


(c) Biodiesel Engine's Ultrafine Particle

Figure 7 TEM images of (a) carbon black, (b) diesel engine's ultrafine particles and (c) biodiesel engine's ultrafine particles in the operation condition 80% of engine load and 2400 rpm of engine speed.

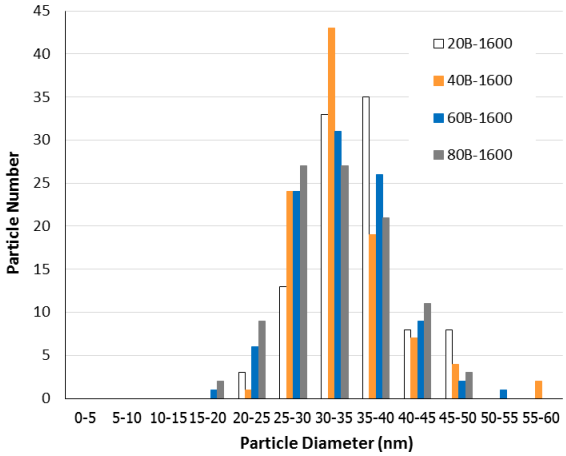


(a) Biodiesel Engine 1600 rpm

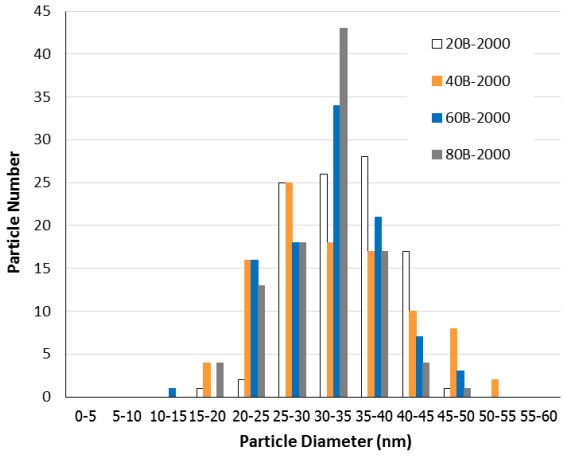


(b) Biodiesel Engine 2000 rpm

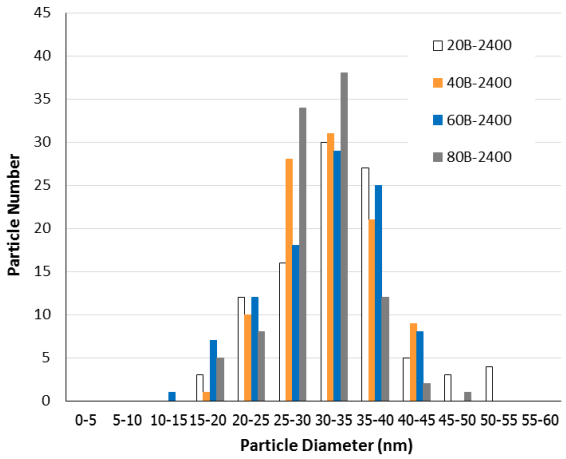


(c) Biodiesel Engine 2400 rpm

Figure 8 Size distributions of biodiesel engine's nanoparticle emissions using TEM image processing method. The engine operation conditions are 20, 40, 60 and 80% of engine load and (a) 1600, (b) 2000 and (c) 2400 rpm of engine speed, respectively.

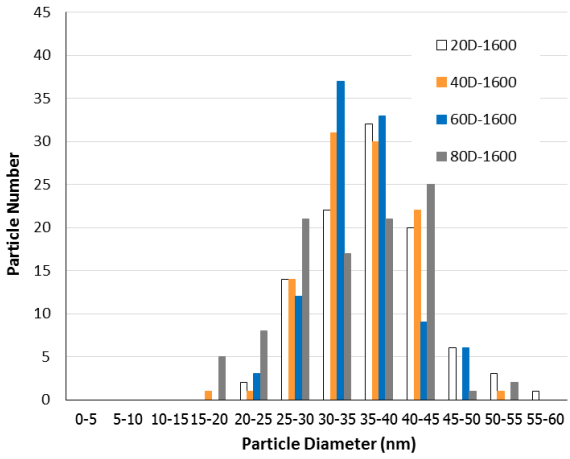


(a) Diesel Engine 1600 rpm

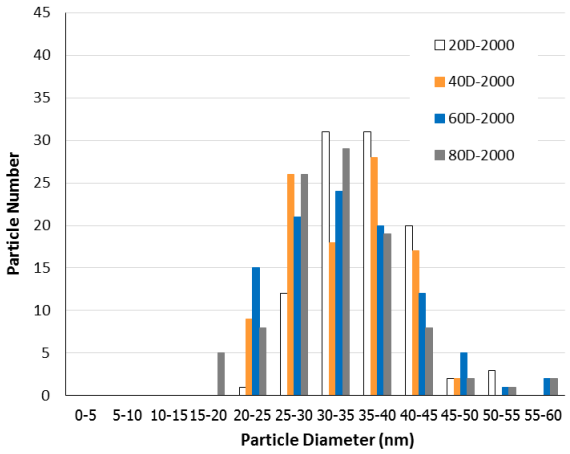


(b) Diesel Engine 2000 rpm

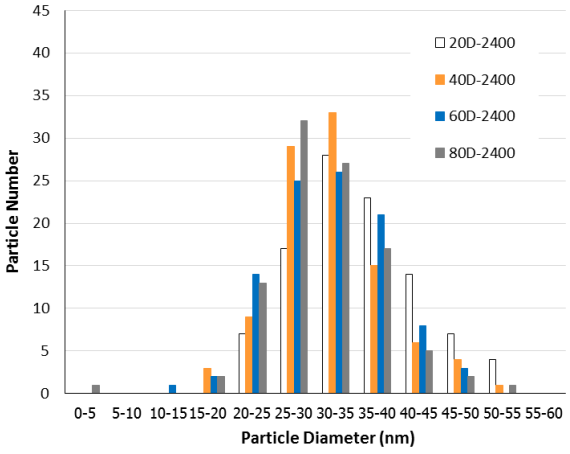


(c) Diesel Engine 2400 rpm

Figure 9 Size distributions of diesel engine's nanoparticle emissions using TEM image processing method. The engine operation conditions are 20, 40, 60 and 80% of engine load and (a) 1600, (b) 2000 and (c) 2400 rpm of engine speed, respectively.

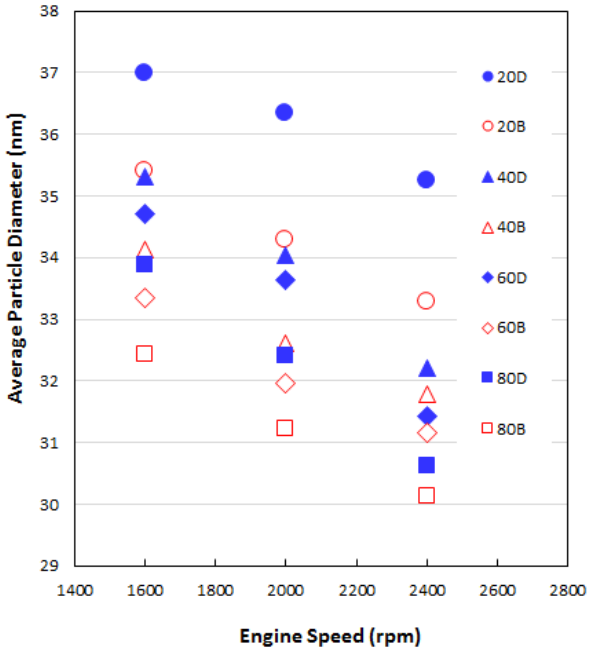


Figure 10 Average particle size of diesel engine's nanoparticles versus biodiesel engine's nanoparticles under 20, 40, 60 and 80% of engine load and 1600, 2000 and 2400 rpm of engine speed using TEM image processing method.

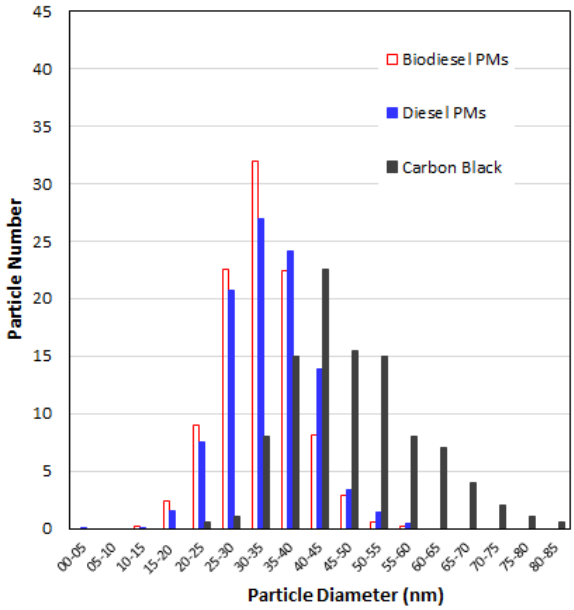


Figure 11 Size distribution of carbon black versus average particle size distribution of diesel engine's nanoparticles and biodiesel engine's nanoparticles under 20, 40, 60 and 80% of engine load and 1600, 2000 and 2400 rpm of engine speed using TEM image processing method.

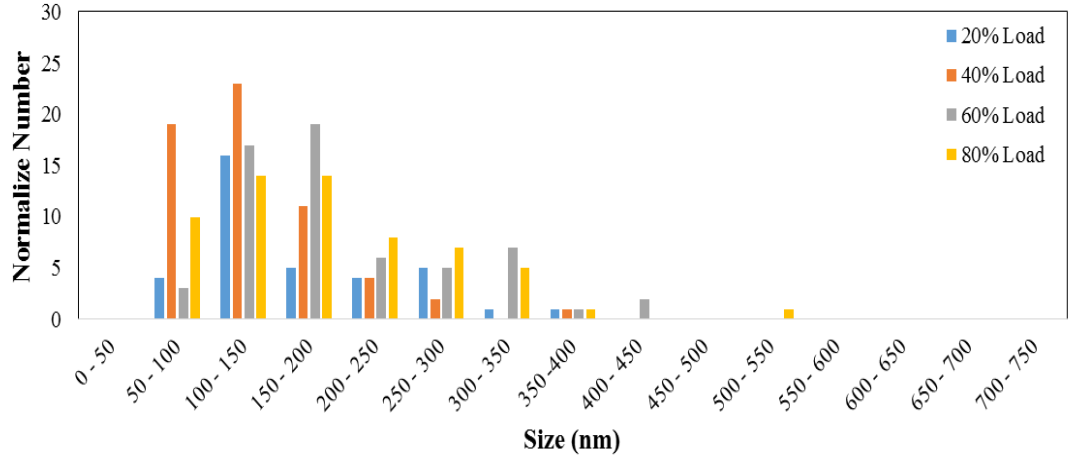


(a) Biodiesel Engine 1600 rpm

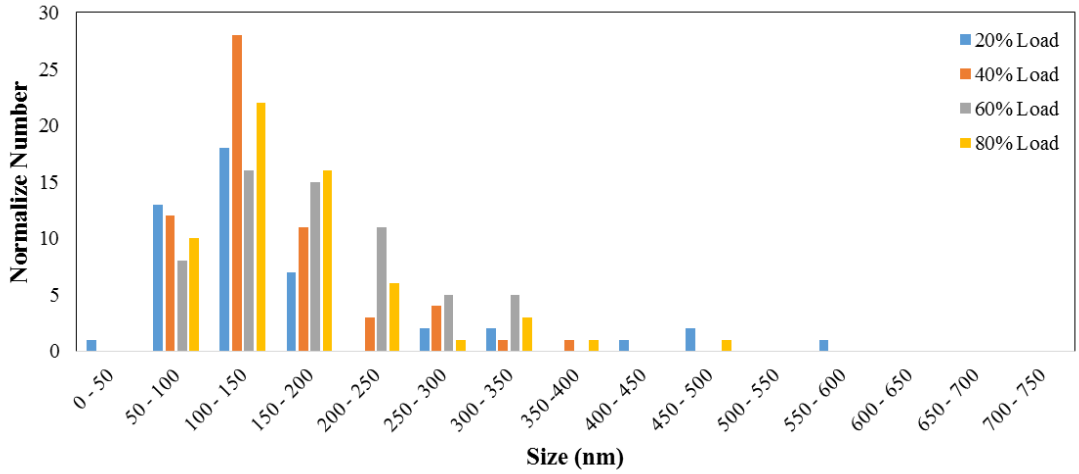


(b) Biodiesel Engine 2000 rpm

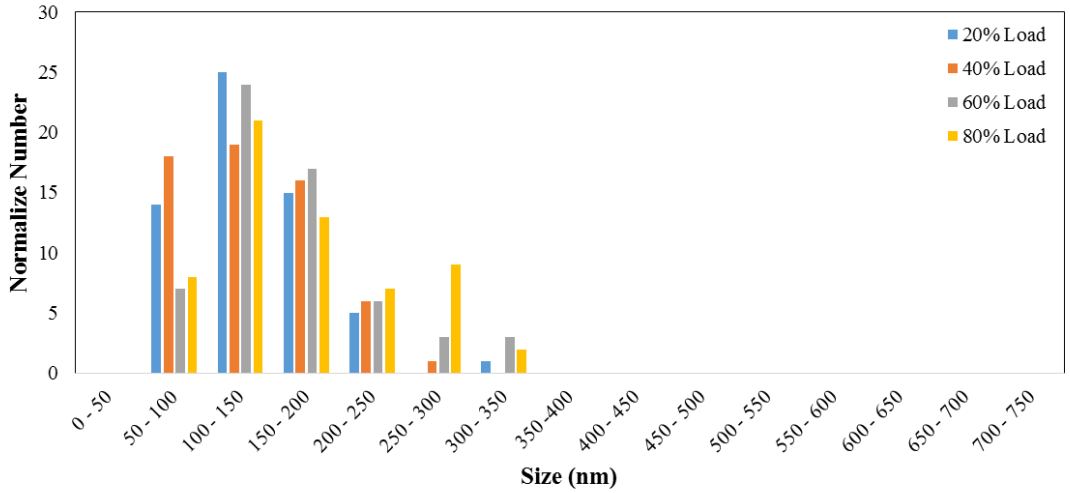


(c) Biodiesel Engine 2400 rpm

Figures 12 Size distribution of agglomerate particulate matter from biodiesel at the engine operation conditions are 20, 40, 60 and 80% of engine load and (a) 1600, (b) 2000 and (c) 2400 rpm of engine speed, respectively.

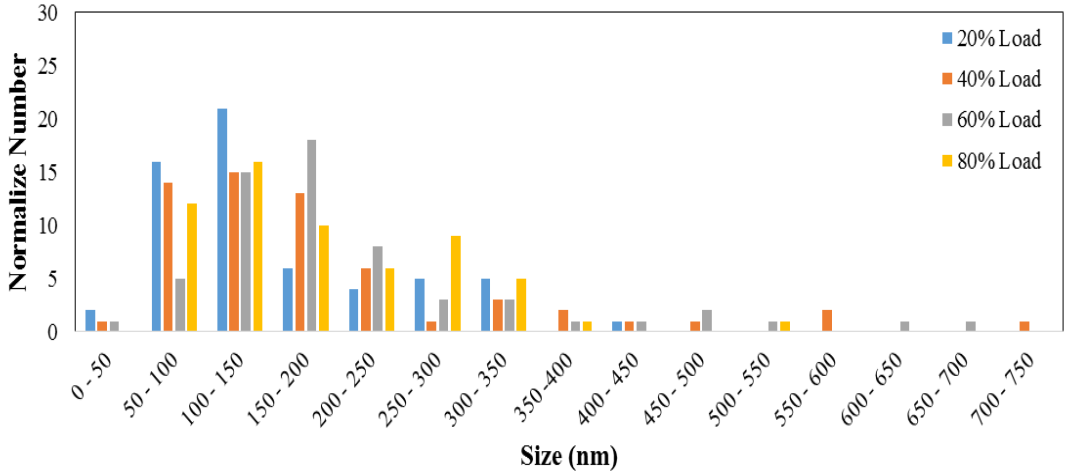


(a) Diesel Engine 1600 rpm

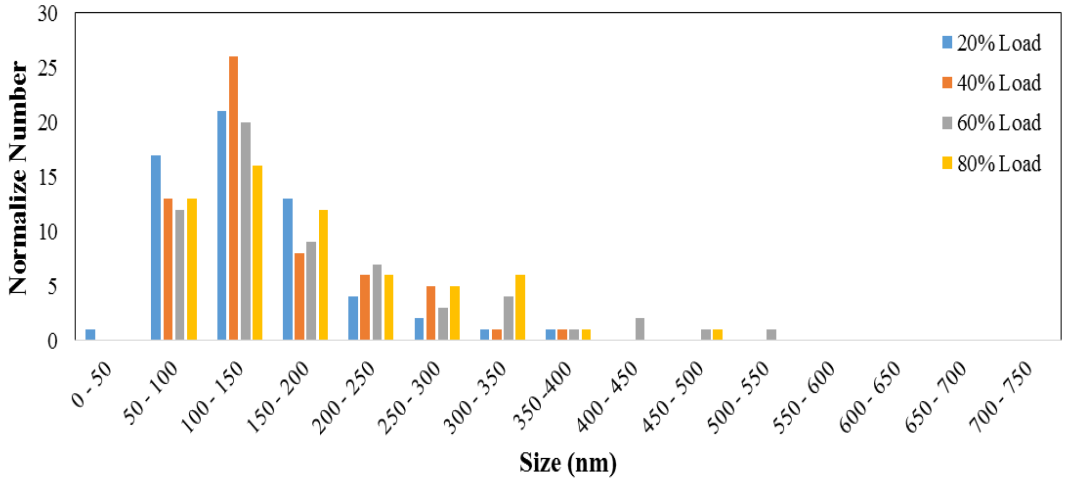


(b) Diesel Engine 2000 rpm

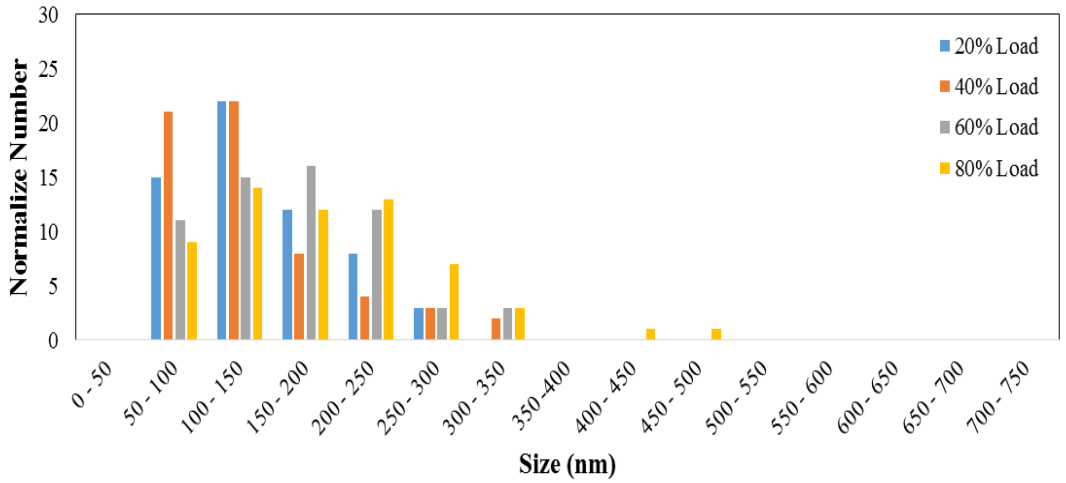


(c) Diesel Engine 2400 rpm

Figures 13 Size distribution of agglomerate particulate matter from diesel at the engine operation conditions are 20, 40, 60 and 80% of engine load and (a) 1600, (b) 2000 and (c) 2400 rpm of engine speed, respectively.

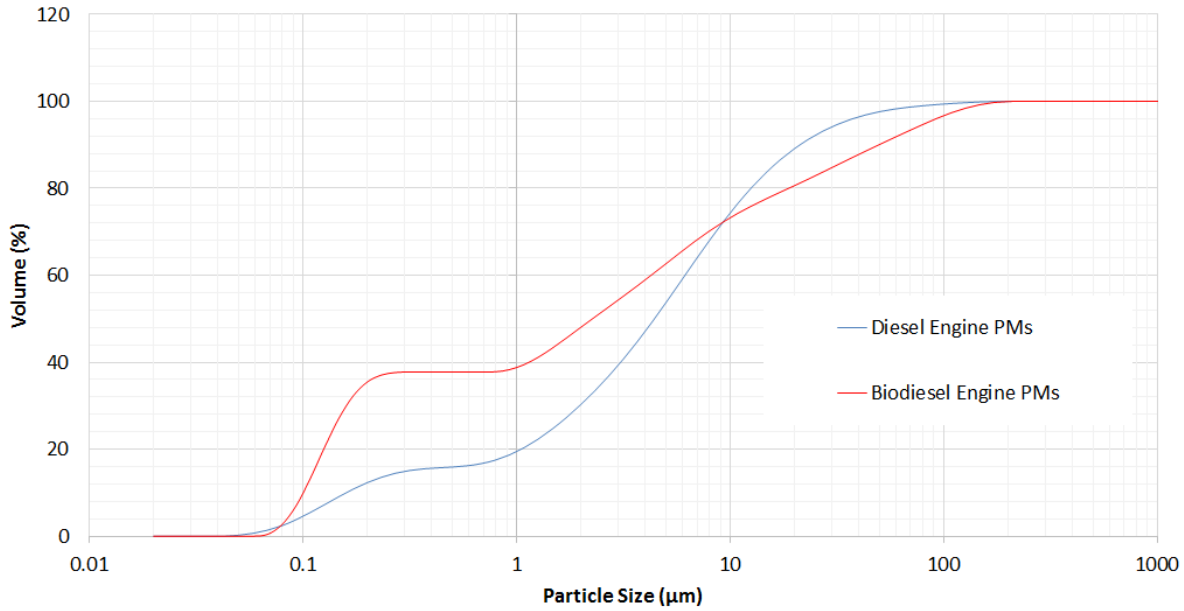


Figures 14 Cumulative size distribution of agglomerate particulate matter from biodiesel and diesel at the engine operation condition 80% of engine load and 2400 rpm of engine speed using laser diffraction technique.

**Particulate Matters Oxidation Kinetics**

Figures 15 show mass conversions of carbon black, diesel engine's PMs and biodiesel engine's PMs oxidation with pure air on DPF powders using TGA isothermal method in the condition of (a) 500, (b) 550 and (c) 600 °C, respectively. It was clearly seen that biodiesel engine's PMs were oxidized faster than diesel engine's PMs. Engine's PMs could be oxidized fastest in the condition of 600 °C and slowest in the condition of 500 °C for both of carbon black and engine's PMs. Absolutely, engine's PMs oxidation rate is higher than carbon black. Figure 16 shows Arrhenius plots of PMs oxidation rate on DPF powders. PMs oxidation rate of 20-40%, 40-60%, 60-80% burned fraction of all cases were clearly observed. The slope of carbon black is higher than that of engine's PMs. Table 3 shows the Apparent activation energies of engine's PMs oxidation on conventional cordierite DPF powders with pure air are in the range of 109-131 kJ/mole. The lowest apparent activation energies of biodiesel and diesel engine's PMs oxidation on conventional cordierite DPF powders are 109 and 117 kJ/mole, respectively. This lowest apparent activation energy occurred in 20-40% of mass burned fraction. Whereas, the highest apparent activation energies of 60-80% of biodiesel and diesel engine's PMs mass burned fraction on DPF powders are 131 and 130 kJ/mole, respectively. It was clearly observed that apparent activation energy of pure PMs oxidation are higher (Karin et al., 2015) than that of PMs oxidiation on DPF powder.

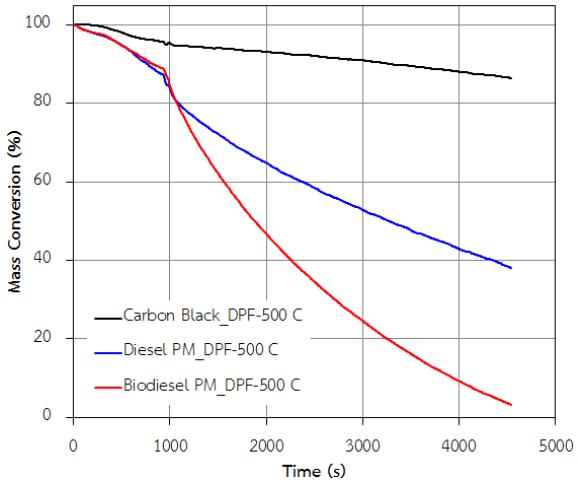


(a) Pure Air Isothermal 500 ºC

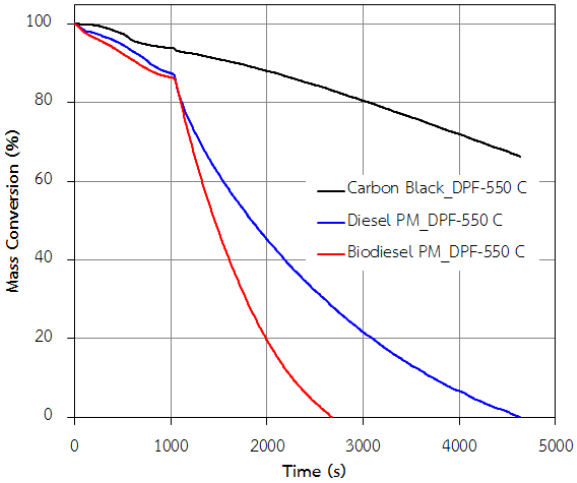


(b) Pure Air Isothermal 550 ºC

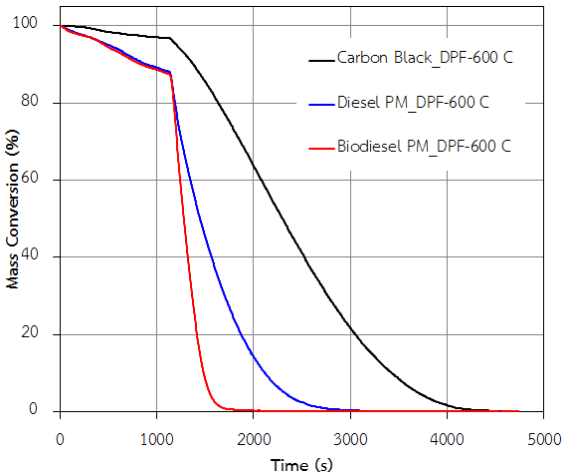


(c) Pure Air Isothermal 600 ºC

Figure 15 Oxidation kinetics of carbon black, diesel engine's PMs and biodiesel engine's PMs on conventional cordierite DPF powders using TGA isothermal method (a) 500 °C, (b) 550 °C and (c) 600 °C with pure air.

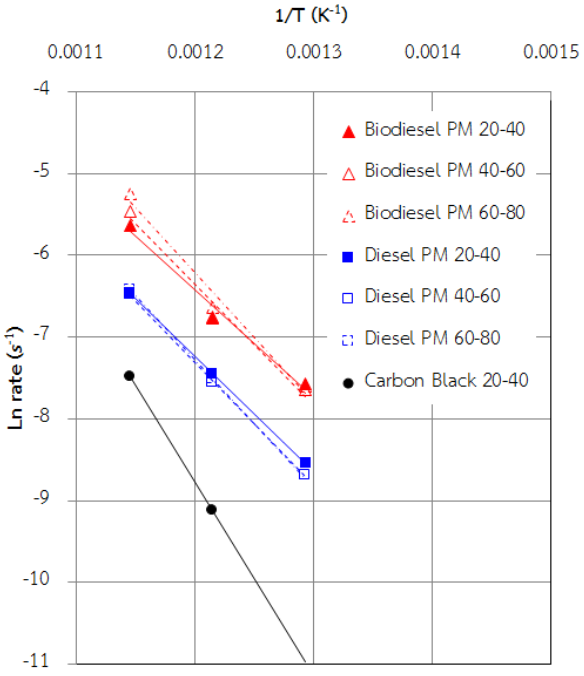


Figure 16 Arrhenius plots of carbon black, diesel engine's PMs and biodiesel engine's PMs oxidation on conventional cordierite DPF powders using TGA isothermal method, 500-550-600 °C with pure air.

Table 3 Calculated apparent activation energies (***Ea***) of engine's PMs oxidize on conventional cordierite DPF powder with pure air

| | | **Apparent Activation Energy *Ea* (kJ/mole)** |
|---|---|---|
| **PMs Oxidize with DPF Powder** | | |
| | **PMs Burned Fraction** | |
| Biodiesel Engine's PMs | | 121±11 |
| | Biodiesel 20-40% burned | 109 |
| | Biodiesel 40-60% burned | 121 |
| | Biodiesel 60-80% burned | 131 |
| Diesel Engine's PMs | | 124±7 |
| | Diesel 20-40% burned | 117 |
| | Diesel 40-60% burned | 124 |
| | Diesel 60-80% burned | 130 |

| **Pure PMs Oxidize without DPF Powder** | |
|---|---|
| Biodiesel Engine's PMs | 152±5 (Karin *et al.*, 2015) |
| Diesel Engine's PMs | 159±6 (Karin *et al.*, 2015) |

Figure 17 (b) shows engine's PMs trapping in the conventional DPF. The trapping duration of diesel PM was approximately 1,600 second. While the trapping duration of biodiesel PM was approximately 3,200 second. The biodiesel PM uses more time duration to trap full the DPF when compare to diesel PM resulting in the pressure during the biodiesel PM trapping in the DPF was increased slower than diesel PM. It was clearly observed that biodiesel PMs were oxidized faster than that of diesel PMs, as shown in Fig. 17 (b).

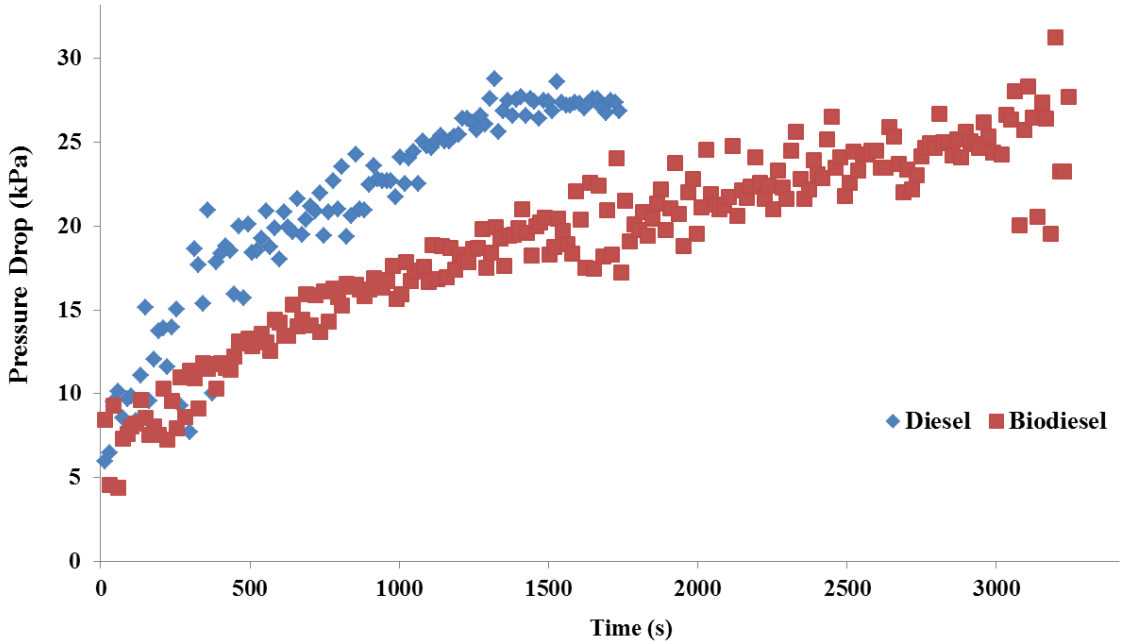


(a) PM Trapping Time

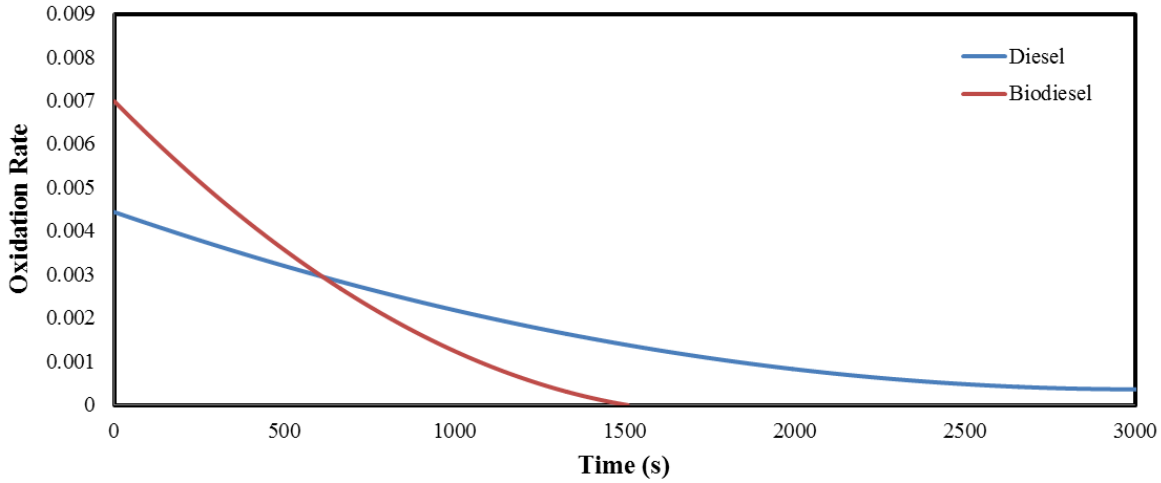


(b) Trapped PM Oxidation

Figure 17 (a) Quantity of diesel engine's PMs and biodiesel engine's PMs by trapping time and (b) trapped PM oxidation kinetics using DPF trapping and oxidation analyzer.

## Conclusion and Discussion

Quantity, morphology and oxidation kinetics of biodiesel engine's PMs were characterized successfully. The quantities of PMs emitted from biodiesel engine are approximately a half of diesel engine's PMs. Average primary nanoparticle sizes of carbon black particles, diesel and biodiesel engine's PMs are approximately 48, 34 and 32 nm, respectively. The quantity and primary particle size of engine's PMs decreased when increasing the engine speed and engine load because of combustion temperature is also automatically increased.

Engine's PMs are easier to oxidize than carbon black nanoparticles because of unburned hydrocarbon and also smaller size of particle. The oxidation rate of biodiesel engine's PMs are higher than that of diesel engine PMs because of unburned bio-oxygenate hydrocarbon and smaller size of particle. Calculated apparent activation energies of biodiesel engine's PM oxidation on conventional cordierite DPF powder are lower than that of diesel engine's PM and carbon black nanoparticles. The apparent activation energies of biodiesel engine's PM and diesel engine's PM oxidation on conventional cordierite DPF powders are 121±11 kJ/mole and 124±7 kJ/mole, respectively.

Oxygen atom included inside oxygenated fuel molecules might promote lower PM oxidation activation energy. However, oxidation rate of particulate matters is strongly related to not only apparent activation energy but also physical impact, such as primary particle size which are strongly related to the reaction order and frequency factor. Smaller primary nanoparticle diameter of biodiesel engine would be an advantage of DPF regeneration process in vehicle application.

## ACKNOWLEDGEMENT

The authors gratefully acknowledge the financial support from Thailand Research Fund (TRF), Thailand.

## REFERENCES


Choi, S., Myung, C. L. and Park, S. (2014). Review on Characterization of Nano-particle Emissions and Morphology from Internal Combustion Engines: Part 2. *International Journal of Automotive Technology*, **15, 2**, 219-227.

Choi, S. and Seong H., (2015). Oxidation Characteristics of Gasoline Direct-Injection (GDI) Engine Soot: Catalytic Effects of Ash and Modified Kinetics Correlation. *Combustion and Flame*, **162**, 2371-2389.

Dacy, P., Costa, P. D., Mellottee, H., Trichard, J. M. and Mariadassou, G. D. (2007). Kinetics of Catalyzed and Non-catalyzed Oxidation of Soot from a Diesel Engine. *Catalysis Today*, **119**, 252-256.

Eastwood, P. (2008). *Particulate Emissions from Vehicles*. SAE International and John Wiley & Sons, Ltd. Pennsylvania.

Fino, D. and Specchai, V. (2008). Review Open Issues in Oxidative Catalysis for Diesel Particulate Abatement. *Powder Technology*, **180**, 64-73.

Hanamura, K., Karin, P., Cui, L., Rubio, P., Tsuruta, T., Tanaka, T. and Suzuki, T. (2009). Micro- and Macroscopic Visualization of Particulate Matter Trapping and Regeneration Processes in Wall-flow Diesel Particulate Filters. *International Journal of Engine Research*, **10**, 305-321.

Ishiguro, T., Takatori Y., Akihama, K. (1997). Microstructure of Diesel Soot Particles Probed by Electron Microscopy: First Observation of Inner Core and Outer Shell. *Combustion and Flame*, **108**, 231-234.

Karin, P., Cui, L., Rubio, P., Tsuruta, T. and Hanamura, K. (2009). Microscopic Visualization of PM Trapping and Regeneration in Micro-Structural Pores of a DPF Wall. *SAE International Journal of Fuels and Lubricants*, **2, 1**, 661-669.

Karin, P. and Hanamura, K. (2010). Particulate Matter Trapping and Oxidation on Catalyst-Membrane. *SAE International Journal of Fuels and Lubricants*, **3, 1**, 368-379.

Karin, P., Songsaengchan, Y., Laosuwan, S., Charoenphonphanich, C., Chollacoop, N., Hanamura, K. (2013). Nanostructure Investigation of Particle Emission by Using TEM Image Processing Method. *Energy Procedia*, **34**, 757-766.

Karin, P., Songsaengchan, Y., Laosuwan, S., Charoenphonphanich, C., Chollacoop, N., Hanamura, K. (2013). Physical Characterization of Biodiesel Particle Emission by Electron Microscopy. *SAE Technical Paper*, 2013-32-9150.

Karin, P., Borhanipour, M., Songsaengchan, Y., Laosuwan, S., Charoenphonphanich, C., Chollacoop, N., Hanamura, K. (2015). Oxidation Kinetics of Small CI Engine's Biodiesel Particulate Matter. *International Journal of Automotive Technology,* **16, 2**, 211-219.

Kittelson, D. B. (1998). Engines and Nanoparticles: A Review. *Journal of Aerosol Science*, 29, 575-588.

Lee, K. O., Seong H. and Choi S. M. (2013). Detailed Analysis of Kinetic Reactions in Soot Oxidation by Simulated Diesel Exhaust Emissions. *Proceeding of the Combustion Institute*, **34**, 3057-3065.

Lee, S., Lee, D., Choi, S. C. (2013). Impact of SME Blended Fuel Combustion on Soot Morphological Characteristics in a Diesel Engine. *International Journal of Automotive Technology*, **14, 5**, 757-762.

Maricq, M. M. (2007). Review Chemical Characterization of Particulate Emissions from Diesel Engine: A Review. *Journal of Aerosol Science*, **38**, 1079-1118.

Myung, C. L., Ko, A. and Park, S. (2014). Review on characterization of nano-particle emissions and PM morphology from internal combustion engines: Part 1. *International Journal of Automotive Technology*, **15**, **2**, 203-218.

Neeft, J. A., Makkee, M. and Moulijn, J. (1996). Diesel Particulate Emission Control. *Fuel Processing Technology,* **47**, 1-69.

Neeft, J. A., Nijhuis, T. X., Smakman, E., Makkee, M. and Moulijn, J. A. (1997). Kinetics of the Oxidation of Diesel Soot. *Fuel*, **76, 12**, 1129-1136.

Oki, H., Karin, P. and Hanamura, K. (2011). Visualization of Oxidation of Soot Nanoparticles Trapped on a Diesel Particulate Membrane Filter. *SAE International Journal of Engines*, **4, 1**, 515-526.

Smith, O. I. (1981). Fundamentals of Soot Formation in Flames with Application to Diesel Engine Particulate Emissions. *Progress in Energy and Combustion Science*, **7**, 275-291.

Soylu, S. (2014). Examination of PN Emissions and Size Distributions of a Hybrid City Bus under Real World Urban Driving Conditions. *International Journal of Automotive Technology*, **15, 3**, 369-376.

Vander Wal, R. L., Yezerets, A. Currier, N. W., Kim, D. H. and Wang, C. H. (2007). HRTEM Study of Diesel Soot Collected from Diesel Particulate Filters. *Carbon*, **45**, 70-77.

Yezerets, A., Currier, N. W., Kin, D. H., Eadler, H. A., Epling, W. S. and Peden, C. H. F. (2005). Differential Kinetic Analysis of Diesel Particulate Matter (Soot) Oxidation by Oxygen using a Step-Response Technique. *Applied Catalysis B: Environmental*, **61**, 120-129.

**Appendix**

---

Example of Diesel Engine Particulate Matter's TEM images

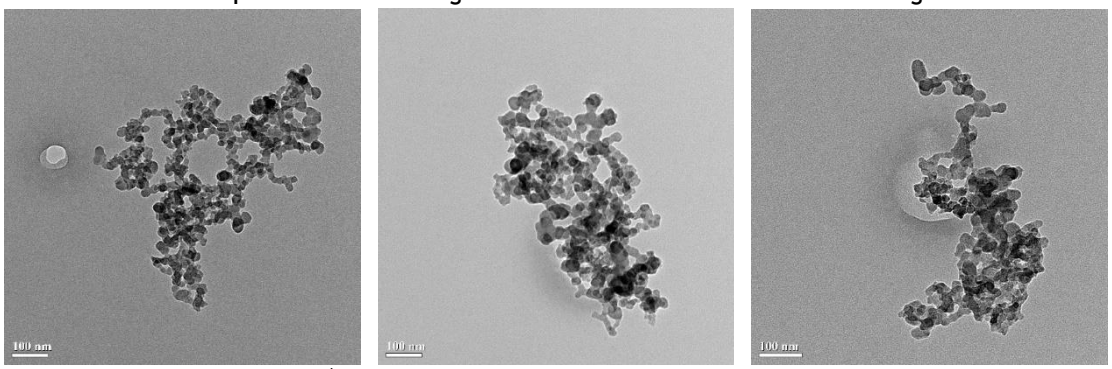

มลพิษอนุภาคดีเซลที่สภาวะโหลด 20 เปอร์เซ็นต์ ความเร็วรอบ 1600 รอบต่อนาที

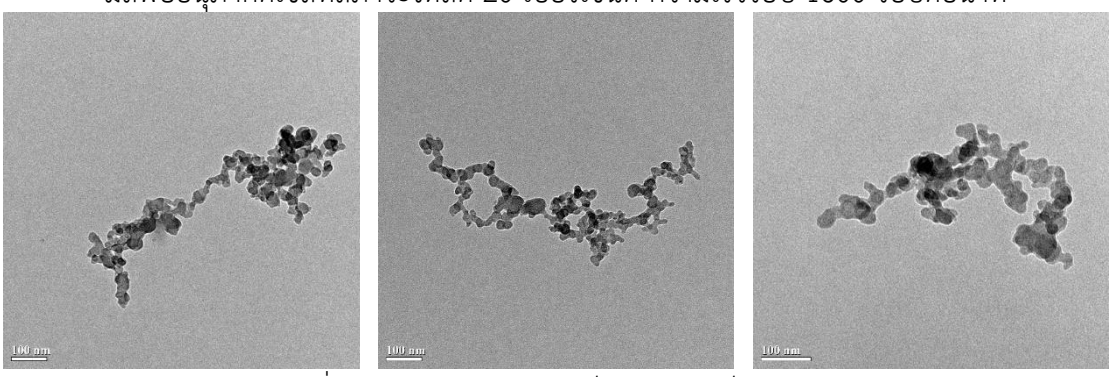

มลพิษอนุภาคดีเซลที่สภาวะโหลด 20 เปอร์เซ็นต์ ความเร็วรอบ 2000 รอบต่อนาที

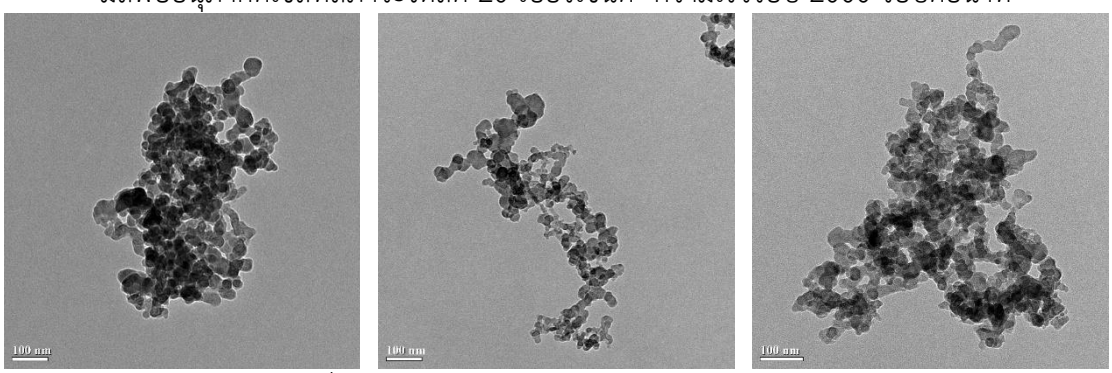

มลพิษอนุภาคดีเซลที่สภาวะโหลด 20 เปอร์เซ็นต์ ความเร็วรอบ 2400 รอบต่อนาที

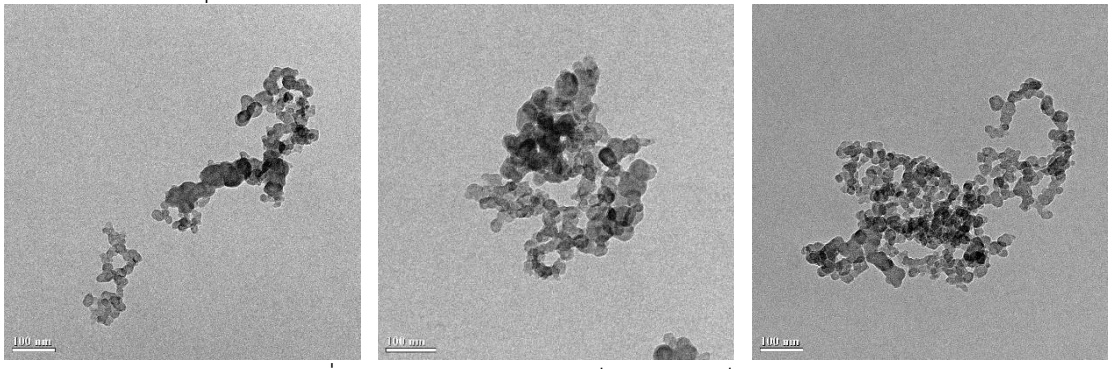

มลพิษอนุภาคดีเซลที่สภาวะโหลด 40 เปอร์เซ็นต์ ความเร็วรอบ 1600 รอบต่อนาที

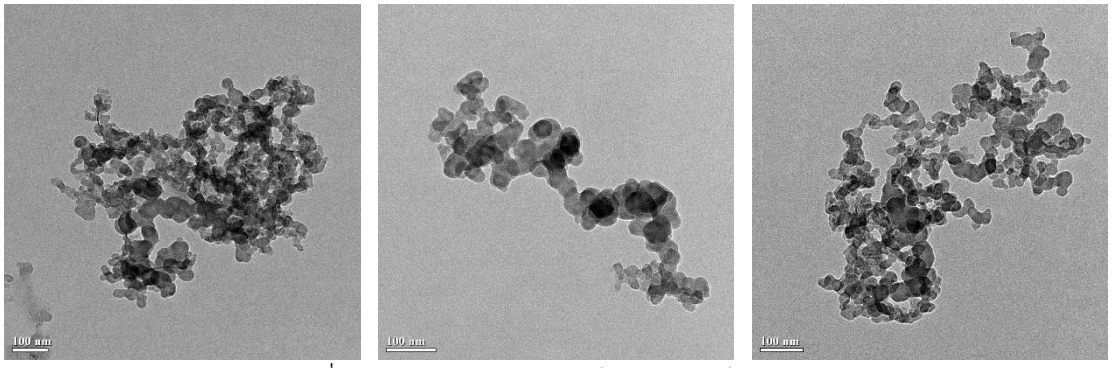

มลพิษอนุภาคดีเซลที่สภาวะโหลด 40 เปอร์เซ็นต์ ความเร็วรอบ 2000 รอบต่อนาที

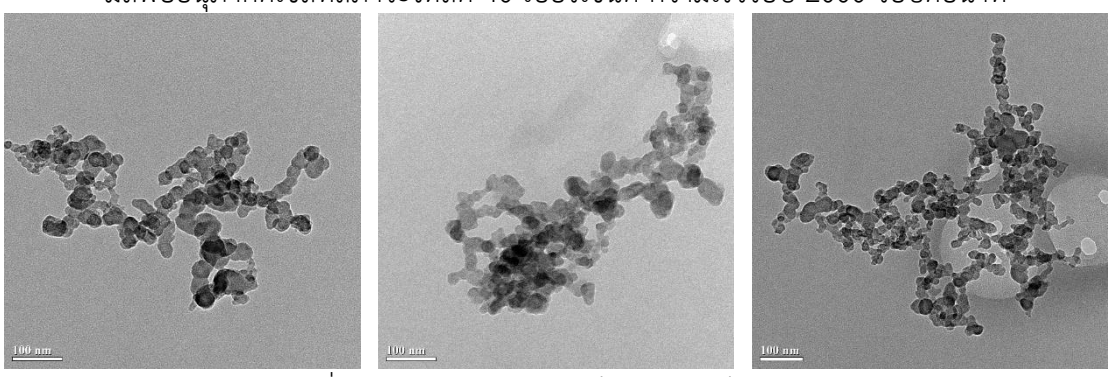

มลพิษอนุภาคดีเซลที่สภาวะโหลด 40 เปอร์เซ็นต์ ความเร็วรอบ 2400 รอบต่อนาที

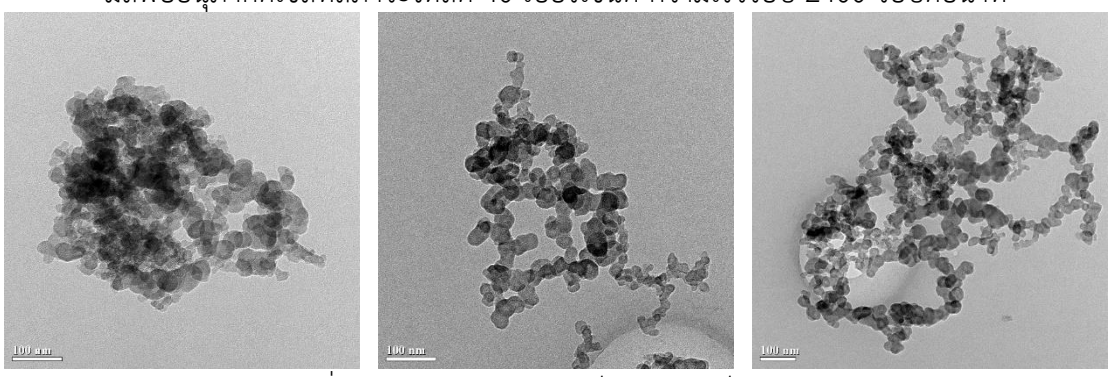

มลพิษอนุภาคดีเซลที่สภาวะโหลด 60 เปอร์เซ็นต์ ความเร็วรอบ 1600 รอบต่อนาที

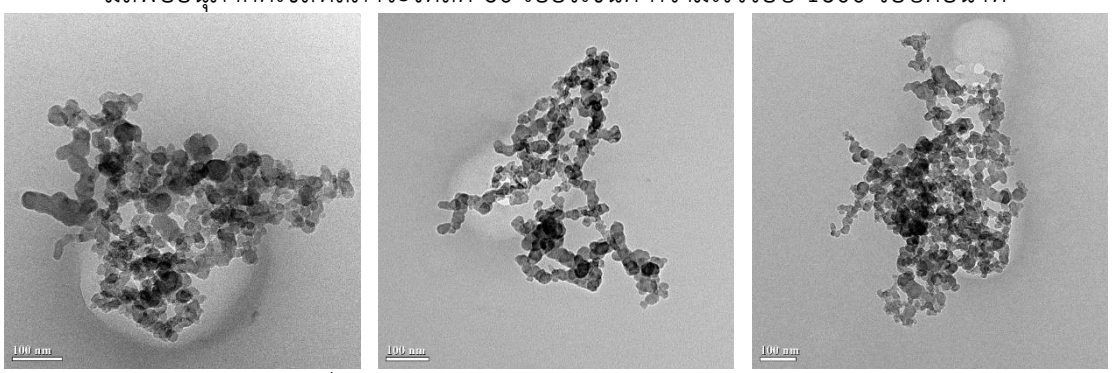

มลพิษอนุภาคดีเซลที่สภาวะโหลด 60 เปอร์เซ็นต์ ความเร็วรอบ 2000 รอบต่อนาที

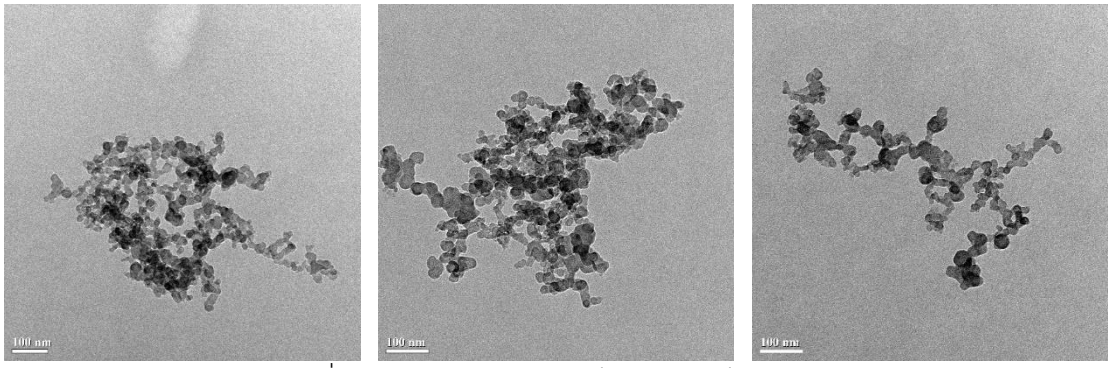


มลพิษอนุภาคดีเซลที่สภาวะโหลด 60 เปอร์เซ็นต์ ความเร็วรอบ 2400 รอบต่อนาที

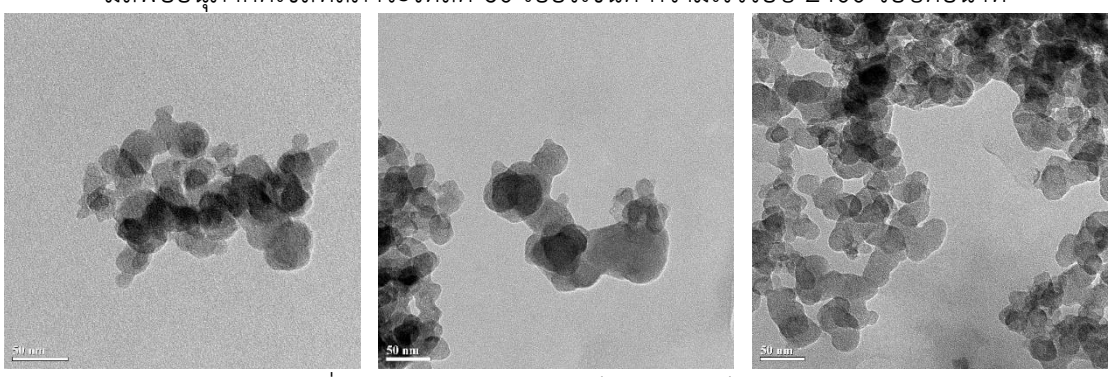


มลพิษอนุภาคดีเซลที่สภาวะโหลด 80 เปอร์เซ็นต์ ความเร็วรอบ 1600 รอบต่อนาที

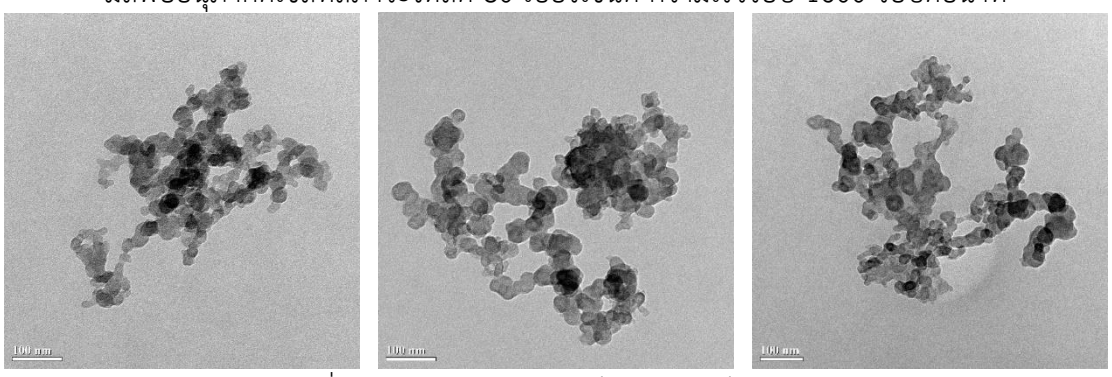


มลพิษอนุภาคดีเซลที่สภาวะโหลด 80 เปอร์เซ็นต์ ความเร็วรอบ 2000 รอบต่อนาที

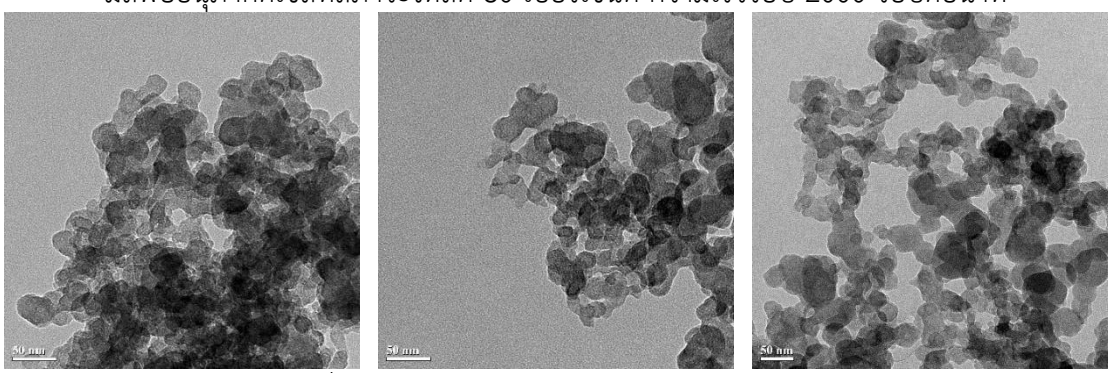


มลพิษอนุภาคดีเซลที่สภาวะโหลด 80 เปอร์เซ็นต์ ความเร็วรอบ 2400 รอบต่อนาที

**Example of Biodiesel Engine Particulate Matter's TEM images**

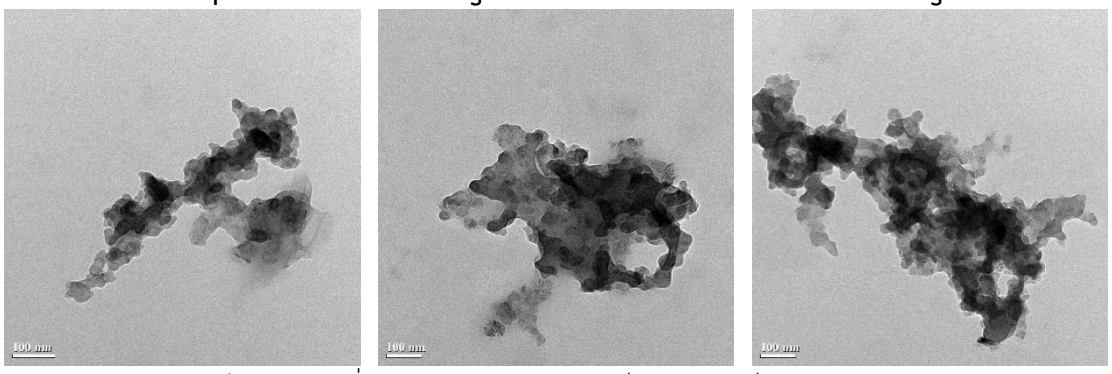

มลพิษอนุภาคไบโอดีเซลที่สภาวะโหลด 20 เปอร์เซ็นต์ ความเร็วรอบ 1600 รอบต่อนาที

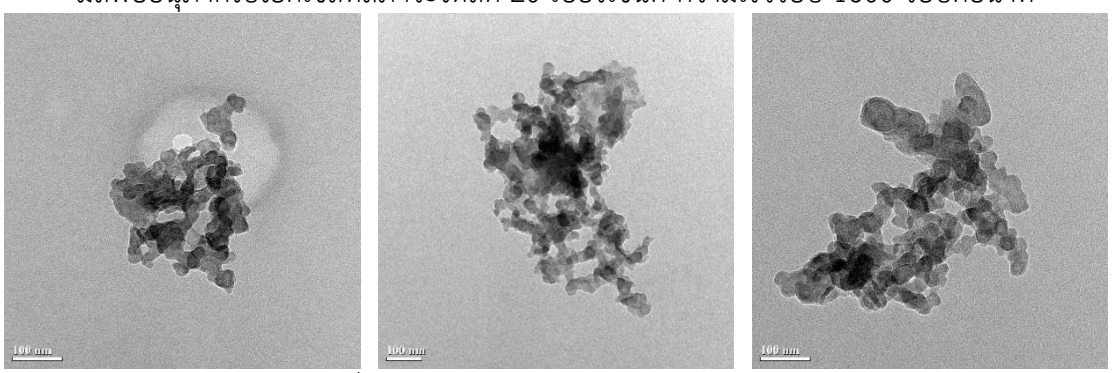

มลพิษอนุภาคไบโอดีเซลที่สภาวะโหลด 20 เปอร์เซ็นต์ ความเร็วรอบ 2000 รอบต่อนาที

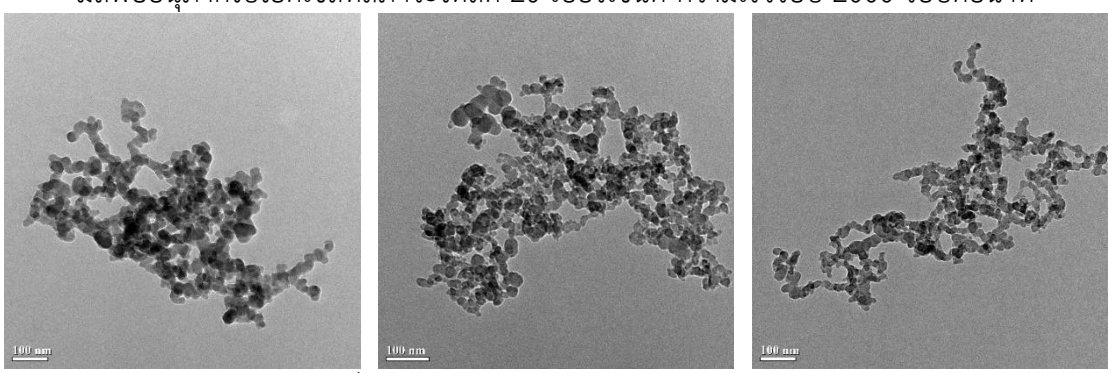

มลพิษอนุภาคไบโอดีเซลที่สภาวะโหลด 20 เปอร์เซ็นต์ ความเร็วรอบ 2400 รอบต่อนาที

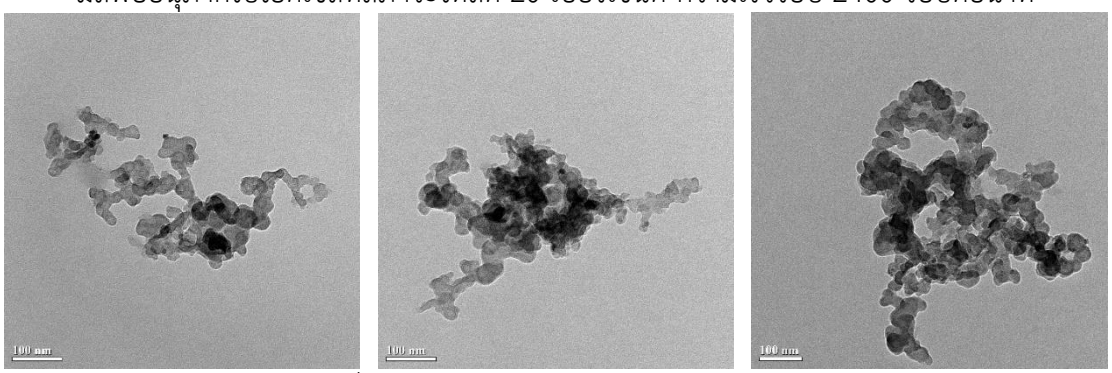

มลพิษอนุภาคไบโอดีเซลที่สภาวะโหลด 40 เปอร์เซ็นต์ ความเร็วรอบ 1600 รอบต่อนาที

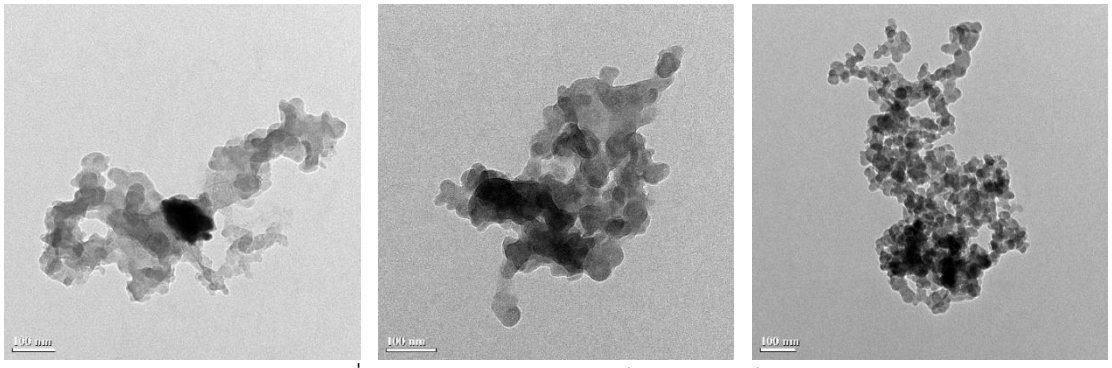

มลพิษอนุภาคไบโอดีเซลที่สภาวะโหลด 40 เปอร์เซ็นต์ ความเร็วรอบ 1600 รอบต่อนาที

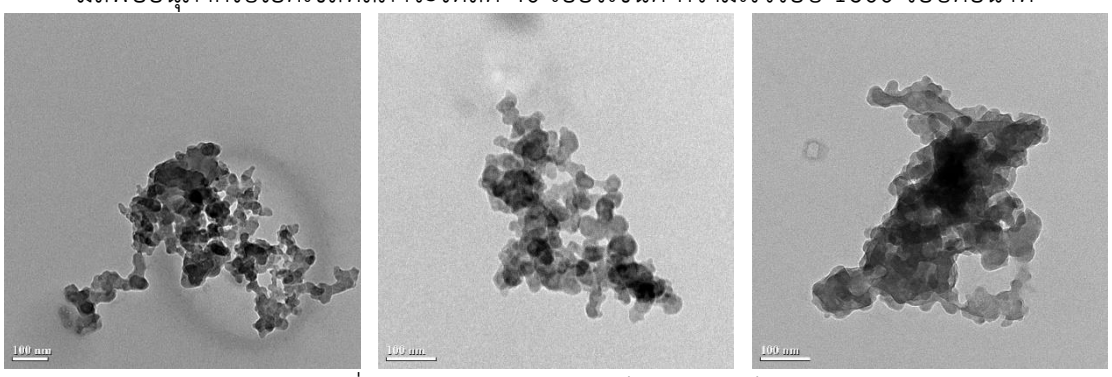

มลพิษอนุภาคไบโอดีเซลที่สภาวะโหลด 40 เปอร์เซ็นต์ ความเร็วรอบ 2400 รอบต่อนาที

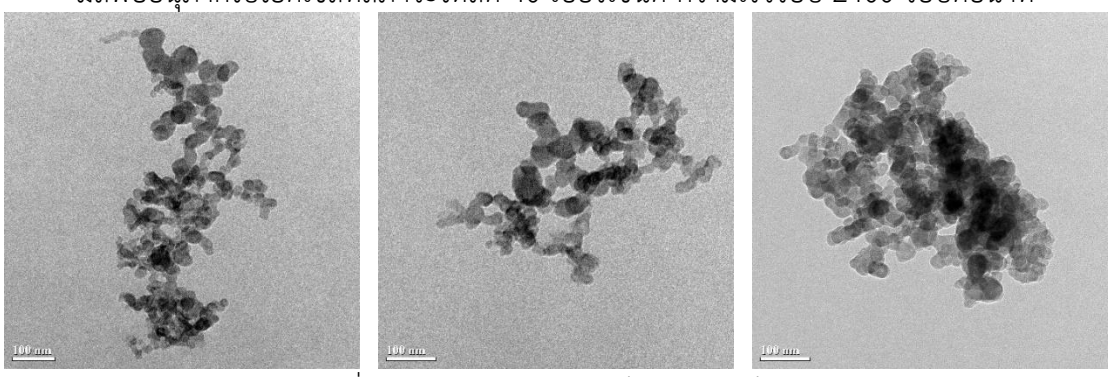

มลพิษอนุภาคไบโอดีเซลที่สภาวะโหลด 60 เปอร์เซ็นต์ ความเร็วรอบ 1600 รอบต่อนาที

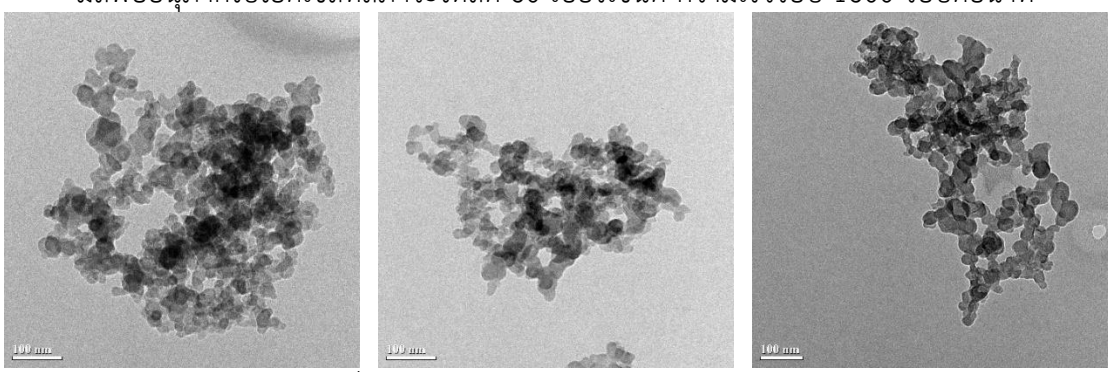

มลพิษอนุภาคไบโอดีเซลที่สภาวะโหลด 60 เปอร์เซ็นต์ ความเร็วรอบ 2000 รอบต่อนาที

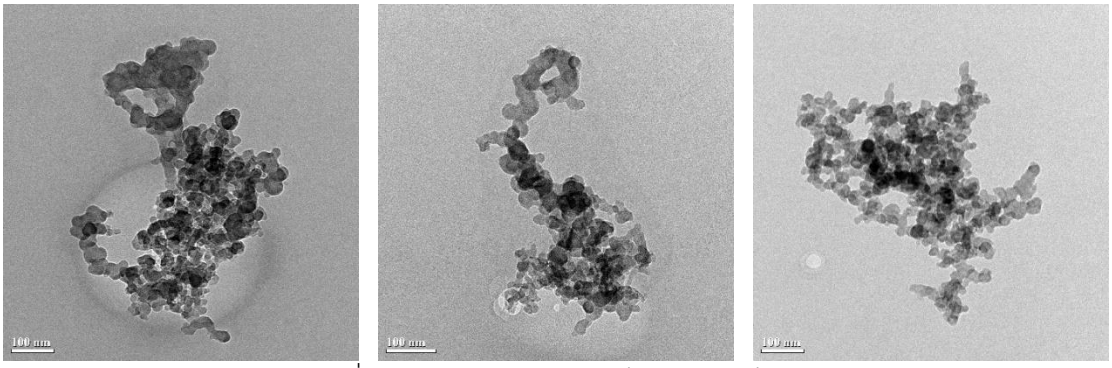

มลพิษอนุภาคไบโอดีเซลที่สภาวะโหลด 60 เปอร์เซ็นต์ ความเร็วรอบ 2400 รอบต่อนาที

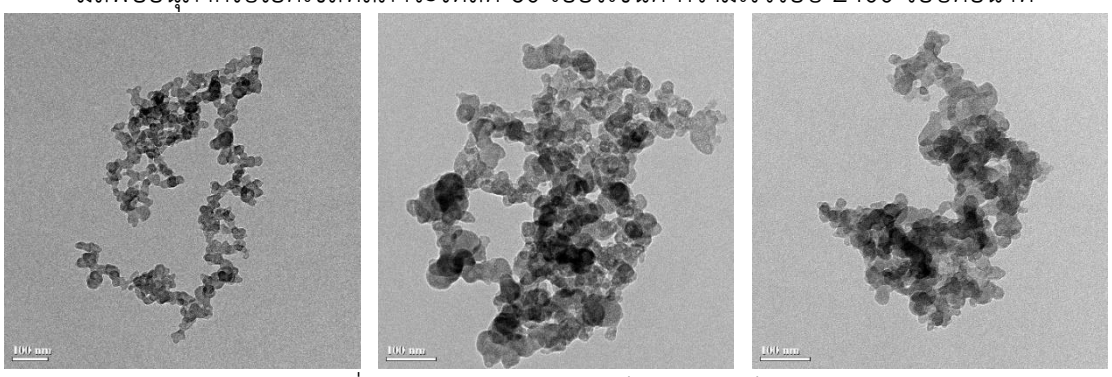

มลพิษอนุภาคไบโอดีเซลที่สภาวะโหลด 80 เปอร์เซ็นต์ ความเร็วรอบ 1600 รอบต่อนาที

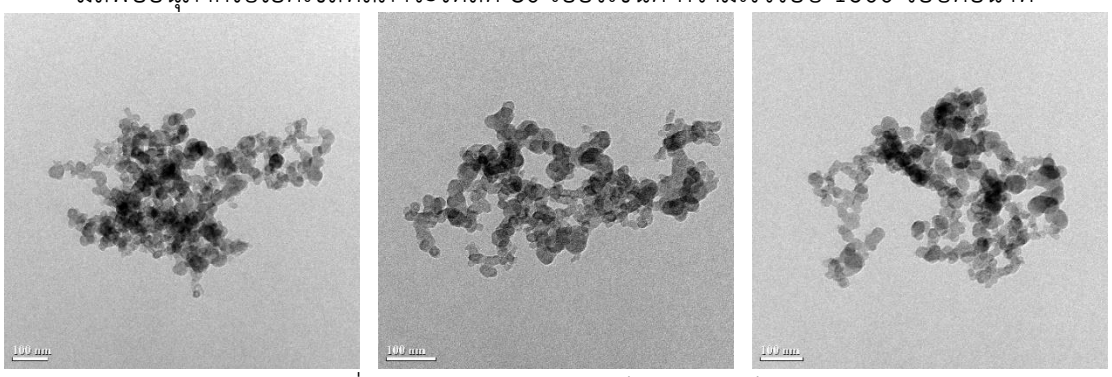

มลพิษอนุภาคไบโอดีเซลที่สภาวะโหลด 80 เปอร์เซ็นต์ ความเร็วรอบ 2000 รอบต่อนาที

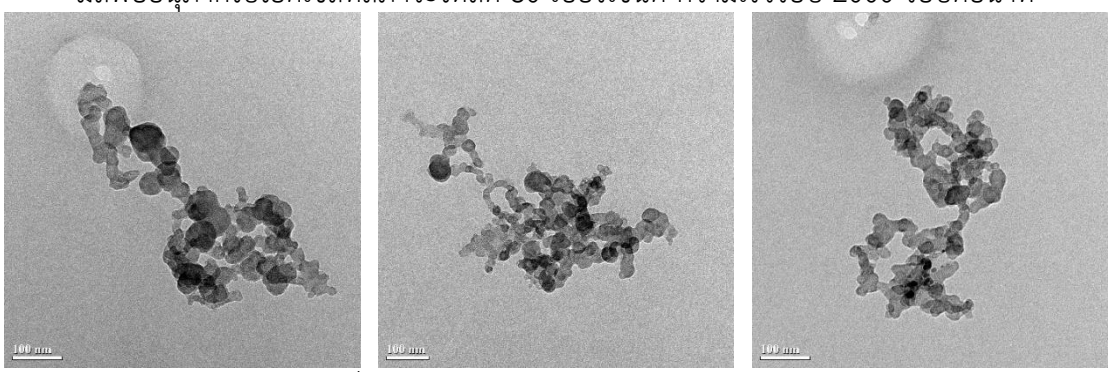

มลพิษอนุภาคไบโอดีเซลที่สภาวะโหลด 80 เปอร์เซ็นต์ ความเร็วรอบ 2400 รอบต่อนาที

Example of Diesel Engine Particulate Matter's SEM images

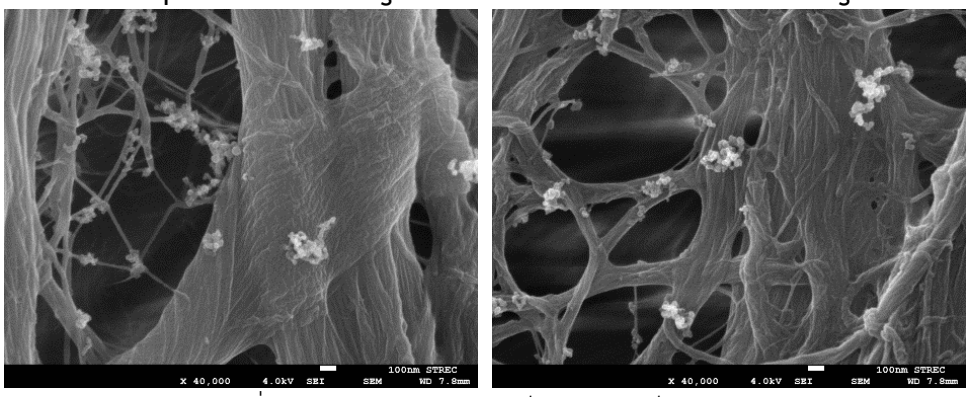


มลพิษอนุภาคดีเซลที่สภาวะโหลด 20 เปอร์เซ็นต์ ความเร็วรอบ 1600 รอบต่อนาที

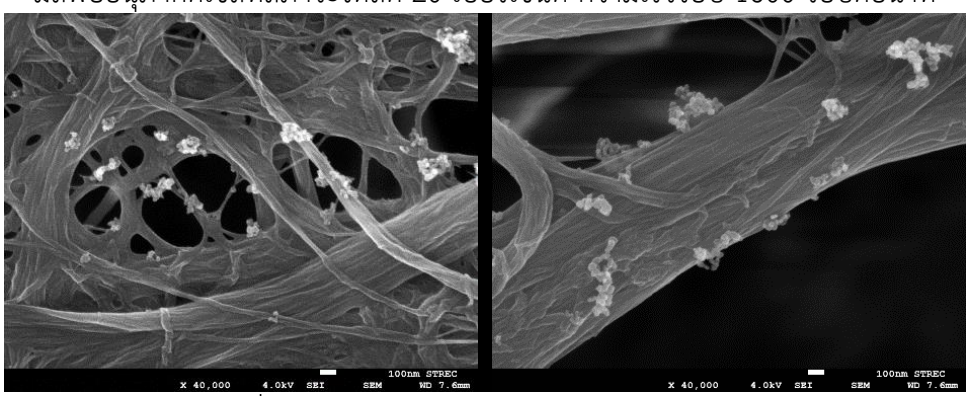


มลพิษอนุภาคดีเซลที่สภาวะโหลด 20 เปอร์เซ็นต์ ความเร็วรอบ 2000 รอบต่อนาที

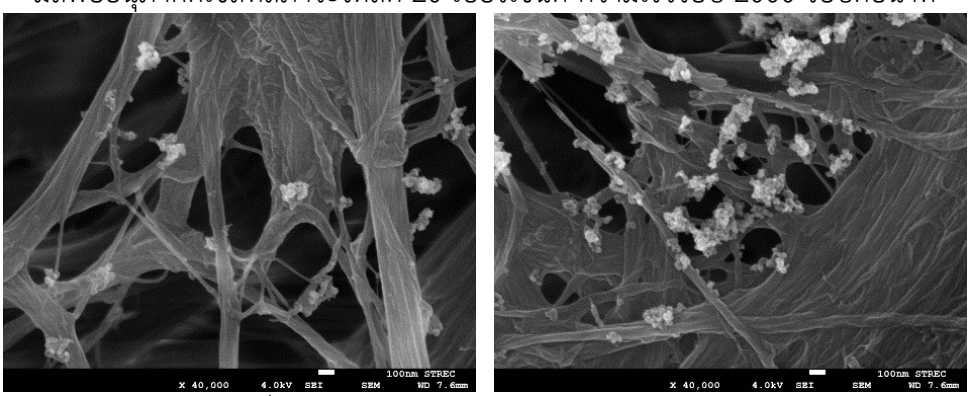


มลพิษอนุภาคดีเซลที่สภาวะโหลด 20 เปอร์เซ็นต์ ความเร็วรอบ 2400 รอบต่อนาที

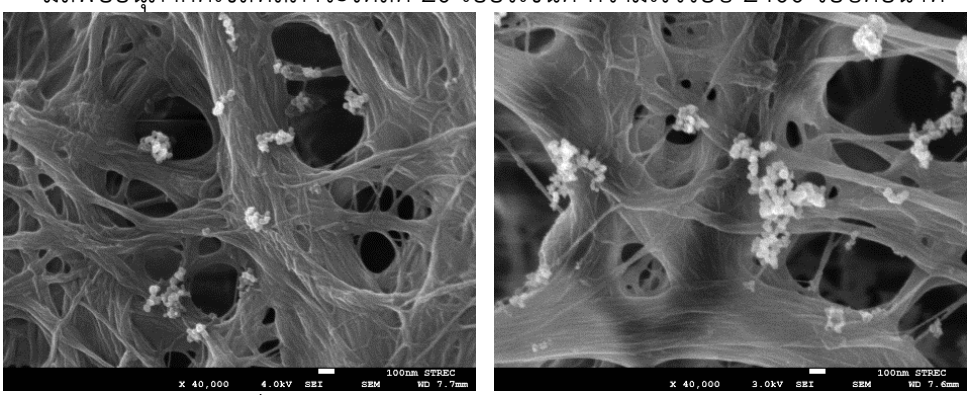


มลพิษอนุภาคดีเซลที่สภาวะโหลด 40 เปอร์เซ็นต์ ความเร็วรอบ 1600 รอบต่อนาที

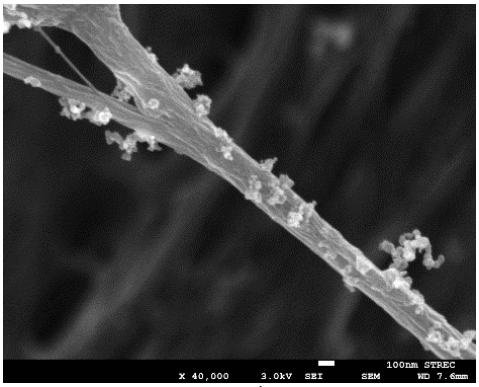

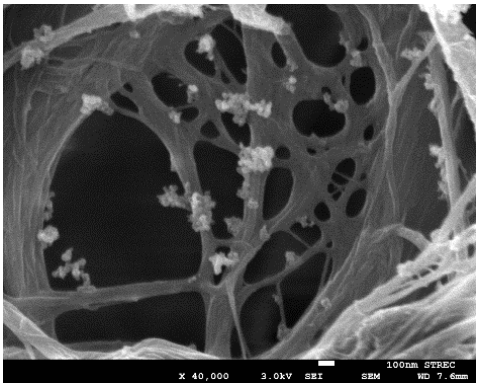


มลพิษอนุภาคดีเซลที่สภาวะโหลด 40 เปอร์เซ็นต์ ความเร็วรอบ 2000 รอบต่อนาที

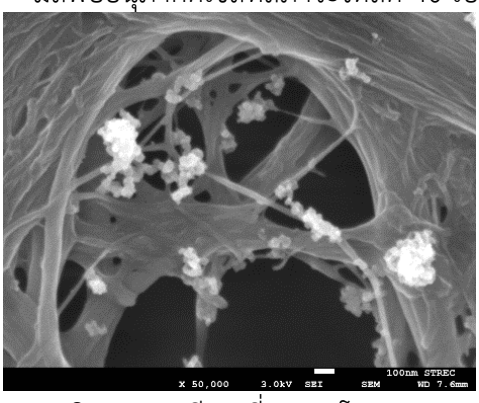

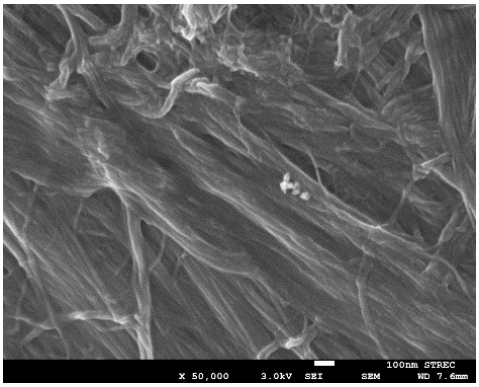


มลพิษอนุภาคดีเซลที่สภาวะโหลด 40 เปอร์เซ็นต์ ความเร็วรอบ 2400 รอบต่อนาที

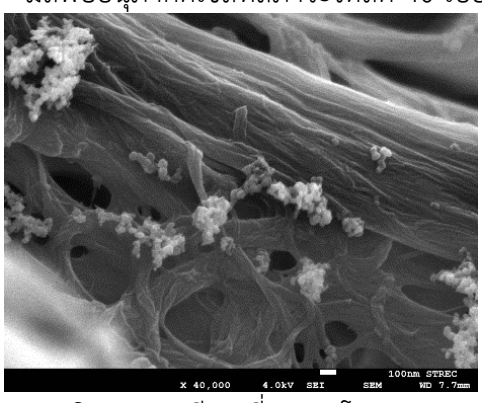

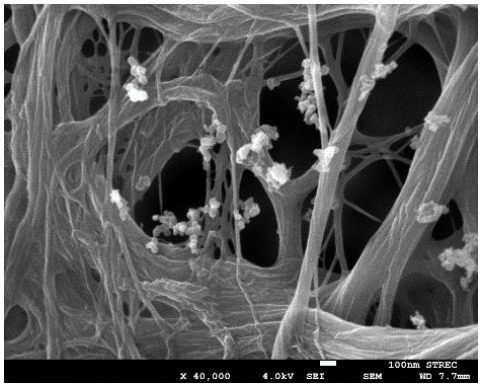


มลพิษอนุภาคดีเซลที่สภาวะโหลด 60 เปอร์เซ็นต์ ความเร็วรอบ 1600 รอบต่อนาที

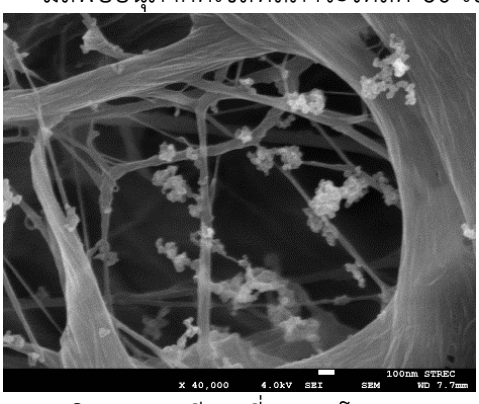

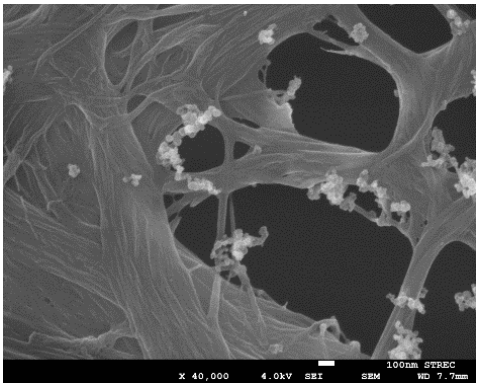


มลพิษอนุภาคดีเซลที่สภาวะโหลด 60 เปอร์เซ็นต์ ความเร็วรอบ 2000 รอบต่อนาที

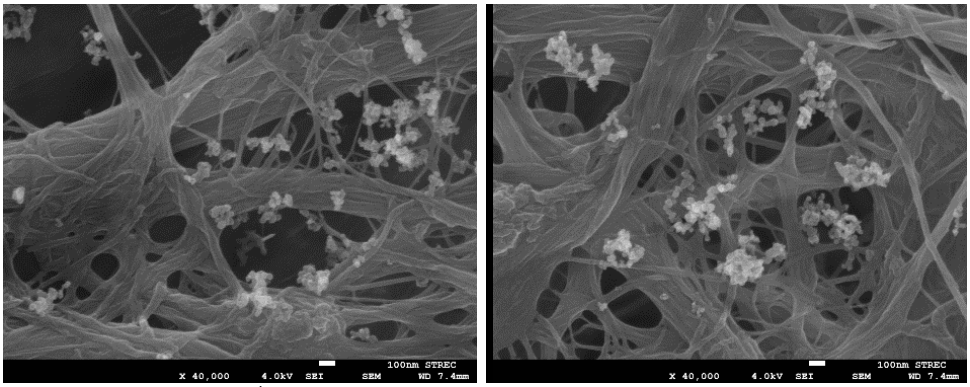


มลพิษอนุภาคดีเซลที่สภาวะโหลด 60 เปอร์เซ็นต์ ความเร็วรอบ 2400 รอบต่อนาที

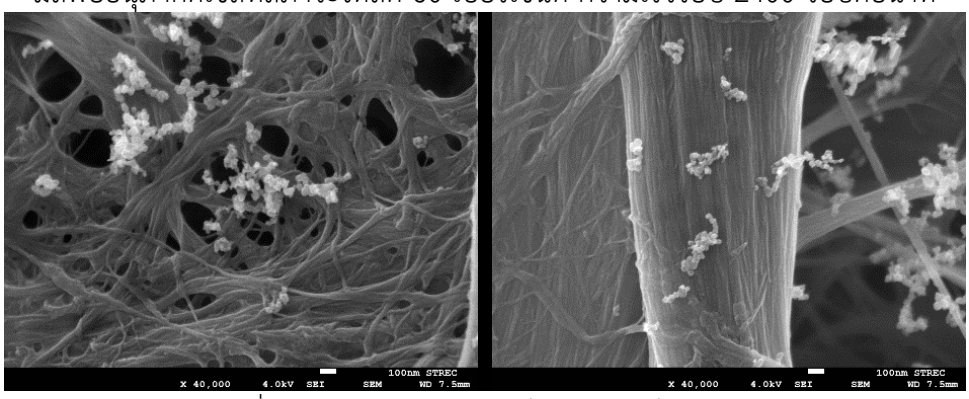


มลพิษอนุภาคดีเซลที่สภาวะโหลด 80 เปอร์เซ็นต์ ความเร็วรอบ 1600 รอบต่อนาที

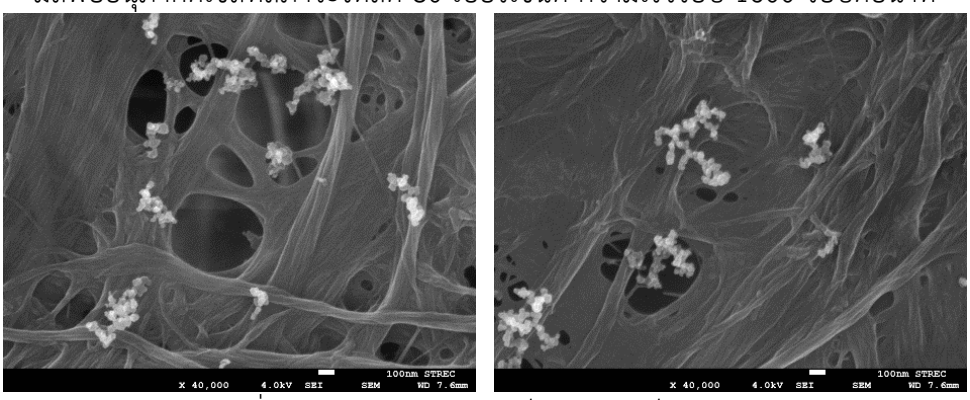


มลพิษอนุภาคดีเซลที่สภาวะโหลด 80 เปอร์เซ็นต์ ความเร็วรอบ 2000 รอบต่อนาที

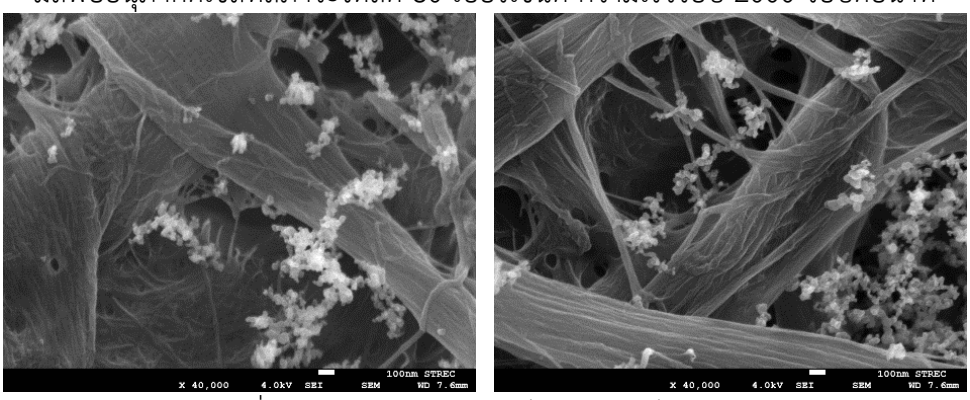


มลพิษอนุภาคดีเซลที่สภาวะโหลด 80 เปอร์เซ็นต์ ความเร็วรอบ 2400 รอบต่อนาที

Example of Biodiesel Engine Particulate Matter's SEM images

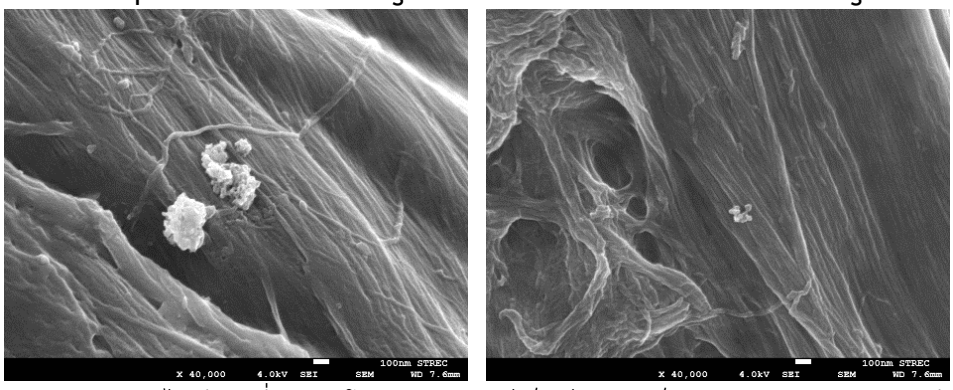


มลพิษอนุภาคไบดีเซลที่สภาวะโหลด 20 เปอร์เซ็นต์ ความเร็วรอบ 1600 รอบต่อนาที

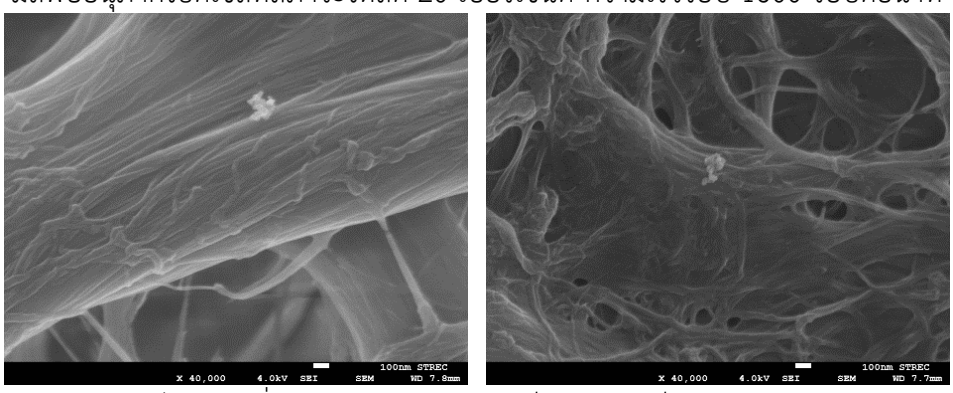


มลพิษอนุภาคไบดีเซลที่สภาวะโหลด 20 เปอร์เซ็นต์ ความเร็วรอบ 2000 รอบต่อนาที

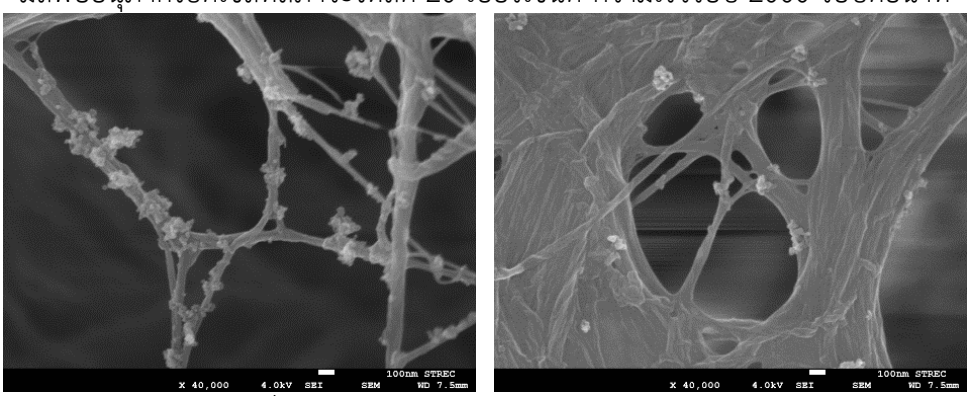


มลพิษอนุภาคไบดีเซลที่สภาวะโหลด 20 เปอร์เซ็นต์ ความเร็วรอบ 2400 รอบต่อนาที

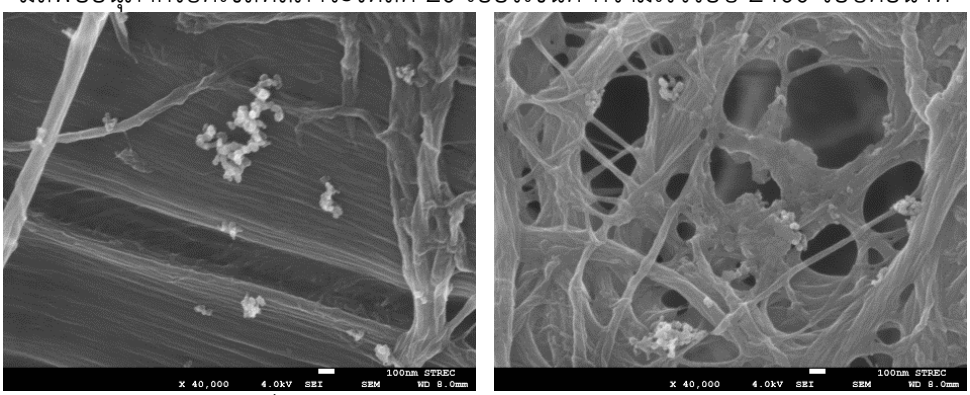


มลพิษอนุภาคไบดีเซลที่สภาวะโหลด 40 เปอร์เซ็นต์ ความเร็วรอบ 1600 รอบต่อนาที

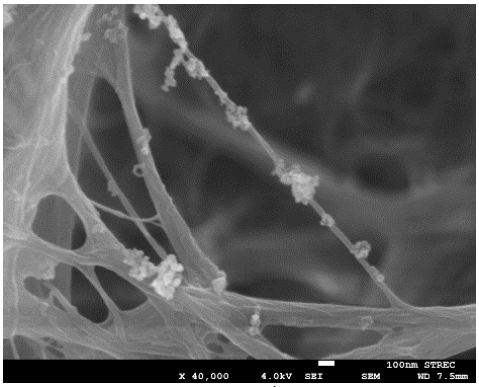

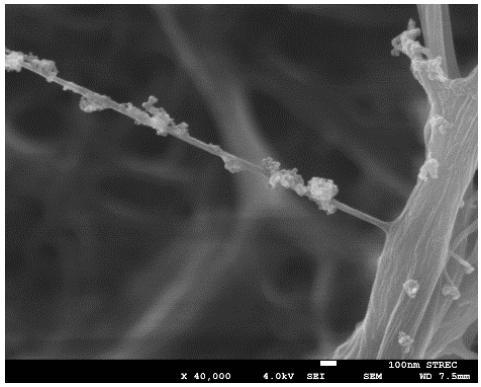


มลพิษอนุภาคไบดีเซลที่สภาวะโหลด 40 เปอร์เซ็นต์ ความเร็วรอบ 2000 รอบต่อนาที

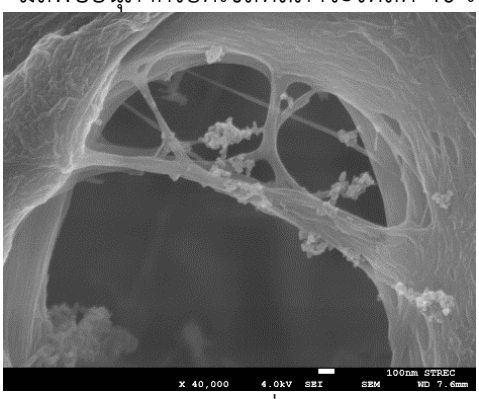

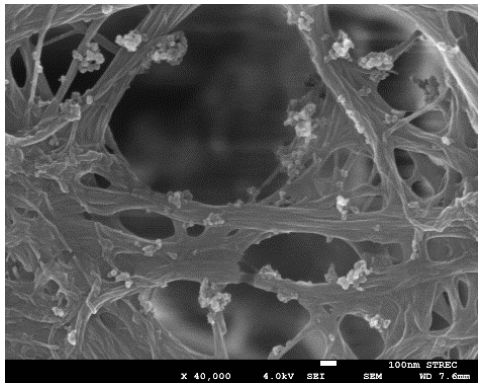


มลพิษอนุภาคไบดีเซลที่สภาวะโหลด 40 เปอร์เซ็นต์ ความเร็วรอบ 2400 รอบต่อนาที

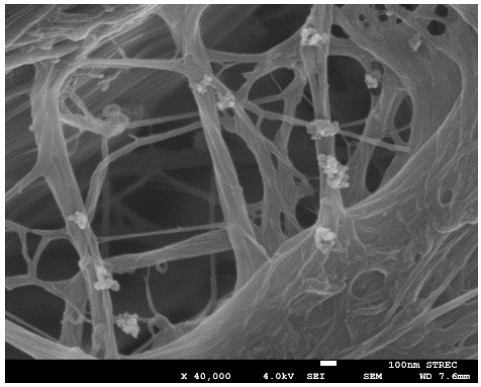


มลพิษอนุภาคไบดีเซลที่สภาวะโหลด 60 เปอร์เซ็นต์ ความเร็วรอบ 1600 รอบต่อนาที

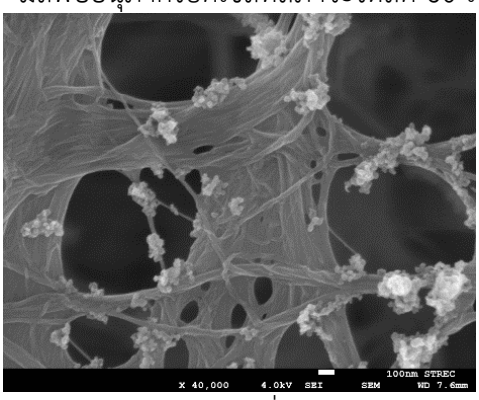

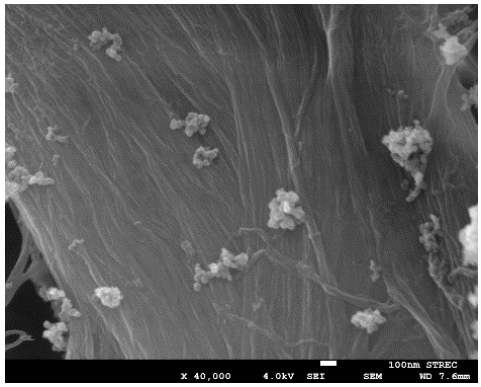


มลพิษอนุภาคไบดีเซลที่สภาวะโหลด 60 เปอร์เซ็นต์ ความเร็วรอบ 2000 รอบต่อนาที

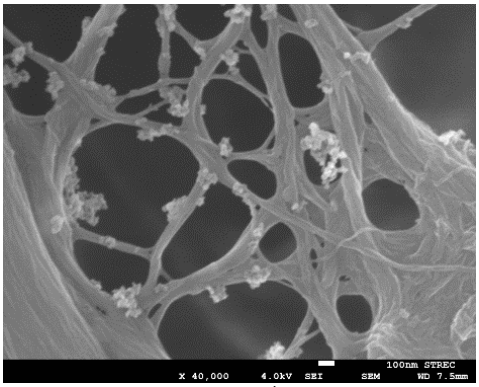

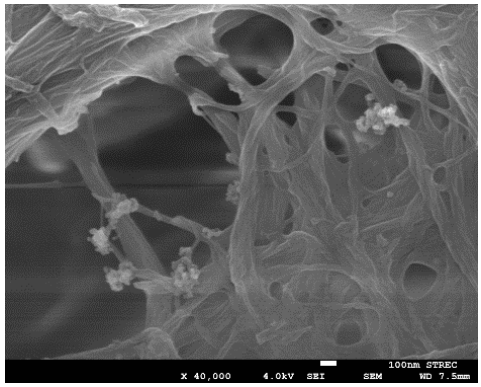


มลพิษอนุภาคไบดีเซลที่สภาวะโหลด 60 เปอร์เซ็นต์ ความเร็วรอบ 2400 รอบต่อนาที

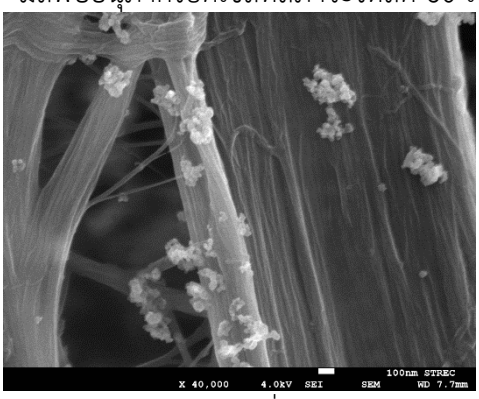

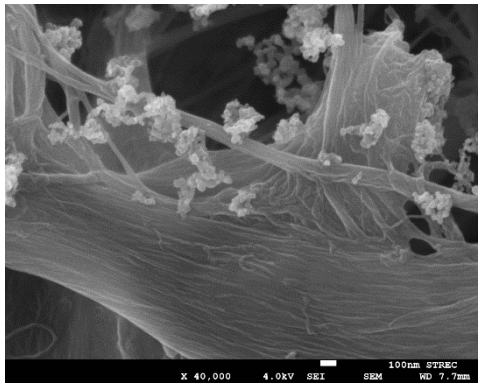


มลพิษอนุภาคไบดีเซลที่สภาวะโหลด 80 เปอร์เซ็นต์ ความเร็วรอบ 1600 รอบต่อนาที

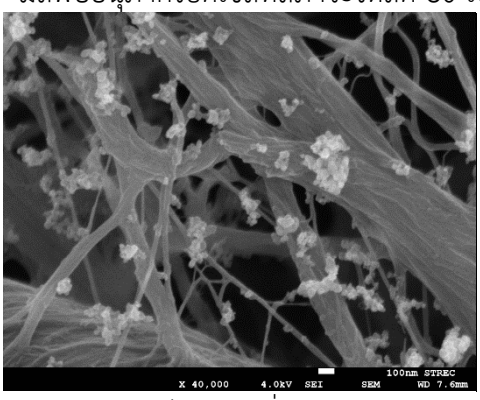

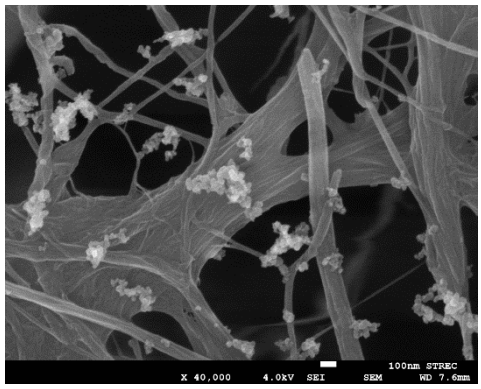


มลพิษอนุภาคไบดีเซลที่สภาวะโหลด 80 เปอร์เซ็นต์ ความเร็วรอบ 2000 รอบต่อนาที

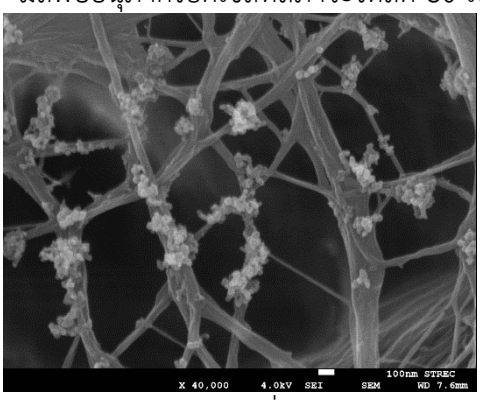

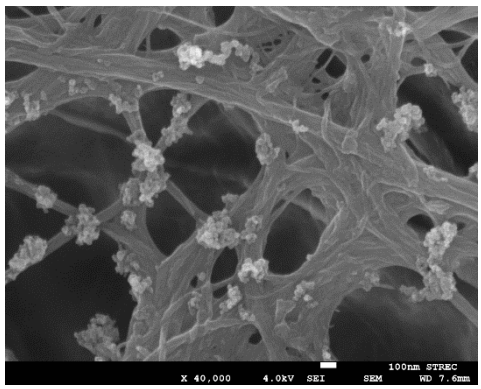


มลพิษอนุภาคไบดีเซลที่สภาวะโหลด 80 เปอร์เซ็นต์ ความเร็วรอบ 2400 รอบต่อนาที

**Output (Acknowledge the Thailand Research Fund)**

---

Output (Acknowledge the Thailand Research Fund)

**Morphology and Oxidation Kinetics of CI Engine's Biodiesel Particulate Matters on Cordierite Diesel Particulate Filters using TGA**, P. Karin, J. Boonsakda, K. Siricholathum, E. Saenkhumvong, C. Charoenphonphanich and K. Hanamura, ***International Journal of Automotive Technology***, 2016 [Accepted, Pre-Publication].

*International Journal of Automotive Technology*, Vol. 00, No. 0, pp. 1−10 (0000)
DOI 10.1007/s12239−017−

pISSN 1229−9138/ eISSN 1976−3832

# MORPHOLOGY AND OXIDATION KINETICS OF CI ENGINE'S BIODIESEL PARTICULATE MATTERS ON CORDIERITE DIESEL PARTICULATE FILTERS USING TGA

P. KARIN[1)*], J. BOONSAKDA[1)], K. SIRICHOLATHUM[1)], E. SAENKHUMVONG[2)], C. CHAROENPHONPHANICH[2)] and K. HANAMURA[3)]

[1)]International College, King Mongkt's Institute of Technology Ladkrabang, Bangkok 10520, Thailand
[2)]Faculty of Engineering, King Mongkut's Institute of Technology Ladkrabang, Bangkok 10520, Thailand
[3)]Department of Mechanical and Control Engineering, Tokyo Institute of Technology, Tokyo 152-8552, Japan

*(Received 14 January 2016; Revised 26 April 2016; Accepted 16 July 2016)*

**ABSTRACT**−The impact of small compression ignition (CI) engine operation conditions and fuel properties on diesel and biodiesel particulate matters (PMs) quantity using opacity smoke meter is investigated. The biodiesel engine's PMs are around a half of diesel engine PMs under the same engine operation conditions. Morphology of both engine's PMs are also studied using a Scanning Electron Microscopy (SEM), Transmission Electron Microscopy (TEM) and image processing method. The average primary nanoparticle sizes of diesel and biodiesel engine's PMs are approximately 34 nm and 32 nm, respectively. The result shows that engine operation condition and fuel property are strongly impact on the quantity and size distribution of primary nanoparticles emission. PM oxidation kinetics on conventional cordierite Diesel Particulate Filters (DPFs) powders by Thermo-gravimetric analysis (TGA) is also successfully studied. The calculated apparent activation energies of biodiesel engine's PM oxidation on conventional cordierite DPFs powders are lower than that of diesel engine's PM and carbon black because of unburned oxygenated molecule. The calculated apparent activation energy of biodiesel engine's PM and diesel engine's PM oxidize on conventional cordierite DPFs powders with pure air are in the range of 109 ~ 131 kJ/mole and 117 ~ 130 kJ/mole, respectively. It might be expected that smaller primary nanoparticle size of biodiesel engine's PMs and bio-oxygenate unburned hydrocarbon can promote more PM oxidation rate during vehicle's DPF regeneration process.

**KEY WORDS** : Diesel engine, Particulate matter, Biodiesel, Activation energy, Oxidation kinetics

## 1. INTRODUCTION

Particulate matter (PMs) must be removed from the exhaust gas emitted from internal combustion engines (ICEs) to protect the human health. Physical and chemical PMs characterization methods for both of spark ignition (SI) and compression ignition (CI) engines under various vehicle certification cycles and real-world driving conditions are reviewed (Choi *et al*., 2014). Physical properties of engine's PMs have been reported by several researchers. The formation of PMs is through to take place via a number of elemental steps: pyrolysis, nucleation, surface growth and coagulation, aggregation and oxidation. These processes take place on different time scales, ranging from a few microseconds to some milliseconds (Neeft *et al*., 1996).

Surface growth is the process in which the precursor molecules grow from nanoparticles. Simultaneously, another process takes place: coagulation. Small particulates collide and coalesce, forming larger spherical particles. Aggregation or chain-forming coagulation accounts for the formation of the well-known "fractal structure of soot (Eastwood, 2008). The carbon atoms are bonded together in hexagonal face-centered arrays in planes commonly referred to as platelets. Platelets are arranged in layers to form crystallites (Smith, 1981). Diesel engine's PMs consists of two particles: i) fractal-like agglomerates of primary particles, consisting of carbon and traces of metallic ash, and coated with condensed heavier and organic compounds and sulfate, and ii) nucleation particles composed of condensed HCs and sulfate (Maricq, 2007).

Scanning Electron Microscopic (SEM) and Transmission Electron Microscope (TEM) observation of particulate matters have been conducted by several researchers. A primary processed soot particle has two distinct parts: an inner core and an outer shell (Ishiguro *et al*., 1997). Generally, a primary particle has only one core with concentric fringe pattern which is hard to be distinguished as inner core and outer shell of internal combustion engine PMs. Some primary particles were found to have a hollow interior and the outer shell exhibiting evidence of graphitization, with a higher crystalline than the non-

**Corresponding author.* e-mail: kkpreech@staff.kmitl.ac.th

hollowed particles (Vander Wal *et al*., 2007). Size distributions of diesel engine's PMs have been reported by several researchers. Most of the particle mass exists in the accumulation mode in the diameter range of few hundred nanometers. Size definitions for atmospheric particles are PM10, diameter ($D$) < 10 μm; fine particles, $D$ < 2.5 μm; ultrafine particles, $D$ < 0.10 μm; and nanoparticles, $D$ < 0.05 μm or 50 nm (Kittelson, 1998). The particles in the size range from 20 to 200 nm are very sensitive to sudden changes of the engine operation conditions (Soylu, 2014).

The oxidation behavior of PMs has been investigated using Thermo-gravimetric Analysis (TGA) and Temperature Program Oxidation (TPO) to evaluate reaction activity. The fit curve results of reaction order for both oxygen and processed soot, and the activation energies, were defined and reported. The reaction order of soot and pure solid carbon particle are in the range of 0.5 ~ 1 due to complex structure of agglomerate particles. The activation energy ($E_a$) of carbon oxidation is around 150 ~ 170 kJ/mole. However, the reaction order of the engine PMs has broader range than the processed soot due to the various crystalline structure and impurity, and also changes with soot conversion (Neeft *et al*., 1997; Darcy *et al*., 2007; Yezerets *et al*., 2005; Fino and Specchai, 2008, Lee *at al.*, 2013a?; Choi and Seong, 2015; Karin *et al*., 2015).

Diesel engine after-treatment technology that substantially reduces particle emissions is Diesel Particulate Filters (DPFs). The DPF plays an important role in PM trapping and oxidation. These processes involve the most complex behavior of PMs and chemical reaction phenomena. Mechanisms of engine's PM trapping and oxidation on DPF wall surface were successfully clarified via real-time macro-microscopic visualization method (Hanamura *et al*., 2009; Karin and Hanamura, 2010; Oki *et al*., 2011).

The effects of engine technologies, fuels, and engine lubricant oils on PM morphology and chemical compositions are also discussed (Myung *et al*., 2014). Biodiesel fuel engine's PMs were investigated and compared with the conventional diesel fuel. PM diameter size and quantity of biodiesel engine are smaller than that of diesel engine. It might be the effect of oxygenated fuel promotes more completely combustion and makes smaller size exiting (Karin *et al*., 2013a?). In the case of biodiesel fuel engine, especially, measured particle parameters such as single particle size and the radius of gyration were decreased compared to those of conventional diesel fuel (Lee *et al*., 2013b?).

The objectives of the present research are to investigate the impact of biodiesel fuel on morphology and oxidation kinetics of engine's PMs on conventional DPF powders by using TEM and TGA, respectively. PM size distribution and oxidation apparent activation energies would be calculated by using TEM image processing method and Arrhenius plots of PM oxidation kinetics for better understanding and future design of DPF configuration for biodiesel blends diesel engine application.

## 2. METHODOLOGY

### 2.1. Particulate Matters Physical Characteristics

A conventional diesel fuel (B5) and biodiesel fuel derived from palm-olein (B100: TIS 2313-2549) were used in this research, as shown in Table 1. The engine has displacement of 638 $cm^3$ and a rated output of 8.8 kW. The engine is a single cylinder, four strokes and direct injection. The fuel injection pressure was approximately 19.6 MPa. The engine was operated by constant speed of 1600, 1800, 2000, 2200 and 2400 rpm and 0, 20, 40, 60 and 80 % load on the Eddy current engine dynamometer (Tokyo plant ED-60-LC), as shown in Table 2.

Engine's PMs quantity were measured using opacity diesel smoke meter (OKUDA DSM-240), which optically evaluate soot collected on paper filters. The measuring method is light reflection method in the range of 0 % ~ 100 %, ± 3 % of measuring accuracy. In addition, engine exhaust's PM samples were collected using in-house metal-net engine particle emission collector. The particle emission collector is located on exhaust manifoild. Optical microscopy (OLYMPUS BX51), scanning electron microscopy (SEM: EVO MA10), transmission electron microscopy (TEM: JEOL JEM-2010) and ImageJ softwear (http://imagej.net) image processing method were used to characterize diesel and biodiesel engine's PM morphology, nanostructure and primary particle size distribution.

### 2.2. Particulate Matters Chemical Characteristics

Engine's PM samples were collected at 2400 rpm of constant engine speed and 80 % of engine load using in-house metal net engine particle emission collector. PM oxidation kinetics were investigated by using thermo-gravimetric analysis (TGA: METTLER TOLEDO TGA/SDTA851e) method with 0.1 mg sensitivity, 0.1 % accuracy of balance mass and 2 °C of temperature error.

Table 1. Physical and chemical fuels properties.

| Fuel properties | Biodiesel | Diesel |
|---|---|---|
| Cetane number | 70 | 55 |
| Heating value (kJ/kg) | 39,550 | 46,800 |
| Density (kg/$m^3$) | 847.73 | 844.78 |
| Viscosity (cSt) | 4.5 | 3.0 |
| Flash point (°C) | 70 | 64 |
| Carbon fraction | 78 | 82 |
| Chemical formula | $C_{15.3}H_{29.5}O_{1.7}$ | $C_{16.2}H_{32.0}$ |

Table 2. Engine operation conditions.

| Engine load (%) | 0 | 20 | 40 | 60 | 80 | 100 |
|---|---|---|---|---|---|---|
| Torque (Nm) | - | 9.5 | 19 | 28.5 | 38 | 47.5 |

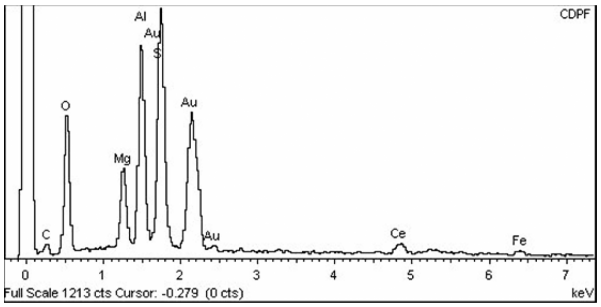


Figure 1. EDS analysis of a conventional cordierite DPF microstructure upstream surface before particulate matters mixing and TGA analysis.

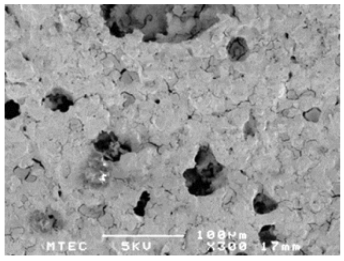

(a) SEM image of DPF upstream surface

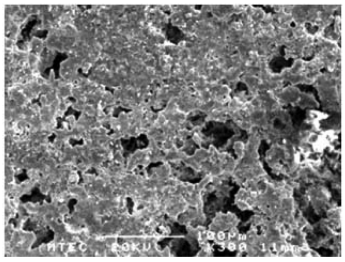

(b) SEM image of DPF wall cross-sectional area

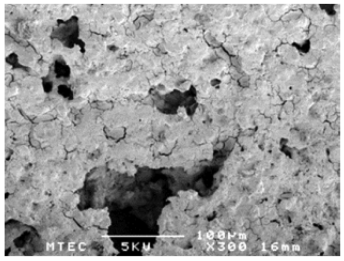

(c) SEM image of DPF downstream surface

Figure 2. SEM images of a conventional cordierite DPF microstructure of (a) DPF upstream surface; (b) DPF wall cross-sectional area; (c) DPF downstream surface, before mixed with carbon black and PMs for TGA analysis.

The conventional cordierite diesel particulate filter (DPF) was milled to be powders. DPF powders were mixed with carbon black (grade: N330), diesel PMs and biodiesel PMs using manual mortar grinding machine. Figure 1 shows conventional DPF upstream surface EDS analysis. It was clearly observed cordierite DPF composition, such as Si, Al, Mg, Fe, O, C, Au, Ce, Fe etc. Figures 2 show SEM images of (a) DPF upstream surface, (b) DPF wall cross-sectional area and (c) DPF downstream surface before mixed with carbon black and PMs using manual mortar grinding machine.

Isothermal method was used to investigate oxidation kinetics of carbon black, diesel PMs and biodiesel PMs on DPF powders. Each mixed sample was tested at three different constant temperature including 500, 550 and 600 $^{o}$C. Nitrogen was used to heat up the sample to desired temperature then pure air is introduced for soot oxidation for one hour. Chemical kinetics of PMs oxidation is studied by using mass conversion behavior from TGA. The chemical reaction rate in Equation 1 can be calculated from the TGA mass conversion curve based on the chemical kinetic in Equation (2). Where ***C*** is PM mass, ***t*** is time, ***n***, ***m*** are the reaction order of PM and oxygen, respectively. The reaction order **n** is assumed to be 2/3 (0.67) as shrinking core model because PM is also assumed to be spherical shape for simplicity. In order to calculate the apparent activation energy (***Ea***) of PM oxidation, the chemical reaction rate constant ***k*** at each temperature in Equation (2) is expressed by Equation (3). Where ***A*** is the frequency factor, ***Ea*** is the activation energy, ***R*** is the gas constant. Finally, the apparent activation energy can be calculated by Equation (4) using the Arrhenius plot.

$$C + O_2 \rightarrow CO_2 \tag{1}$$

$$-\frac{d[C]}{dt} = k[C]^{n}[O_2]^{m} \tag{2}$$

$$k = Ae^{-\frac{E_a}{RT}} \tag{3}$$

$$\ln\left[\frac{-1}{[C]^{n}}\frac{d[C]}{dt}\right] = -\frac{E_a}{RT} + (\ln A + m\ln[O_2]) \tag{4}$$

## 3. RESULTS AND DISCUSSION

### 3.1. Particulate Matters Quantity and Morphology

Figure 3 shows SEM image of biodiesel engine's PM in the condition 80 % of engine load and 2,400 rpm of engine speed, captured by paper filter using smoke meter. Trapped PM10 were clearly observed as shown in white circle. It was clearly observed that PM10 is a group of agglomerated PMs. Morphology of biodiesel's engine PM10 are not significant different from that of diesel's engine.

Figures 4 show quantity of (a) diesel engine's PMs and (b) biodiesel engine's PMs using opacity smoke meter in the condition 20, 40, 60 and 80 % of engine load, 1,600, 1,800, 2,000, 2,200 and 2,400 rpm of engine speed. The result shows that engine's PMs increased with engine load. It might be expected that increasing load or amount of fuel injection resulting in increasing of PMs. Large amount of engine's PMs was clearly observed in both low and high

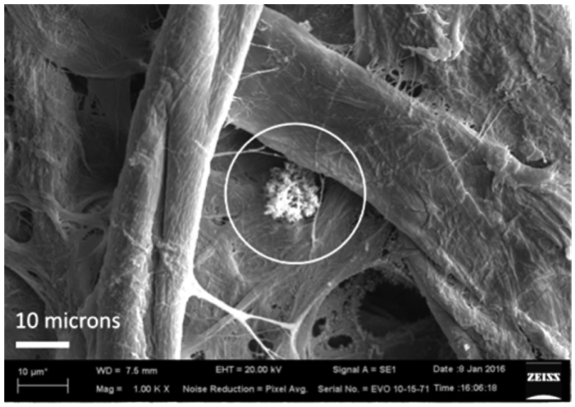


Figure 3. SEM image of biodiesel engine's PM10 in the condition 80 % of engine load and 2,400 rpm of engine speed, captured by glass fiber filters.

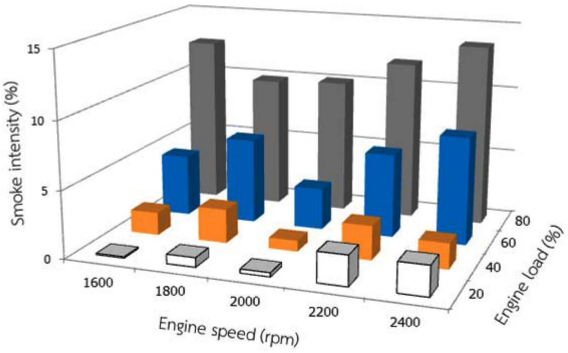


(a) Diesel engine's particulate matters

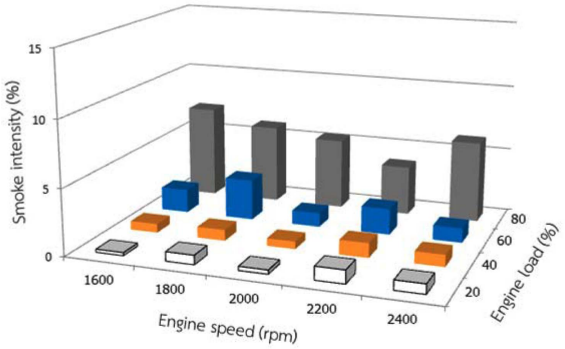


(b) Biodiesel engine's particulate matters

Figure 4. Quantity of (a) Diesel engine's PMs and (b) Biodiesel engine's PMs using opacity smoke meter in each engine load and engine speed operation condition.

engine speed whereas small amount of engine's PMs in the medium engine speed which is the condition of lowest engine energy consumption. Absolutely, the quantities of PMs emitted from biodiesel engine are approximately half of diesel engine because of bio-oxygenate fuel.

Figures 5 show TEM images of biodiesel engine's (a) agglomerate ultrafine particle and (b) primary nanoparticle

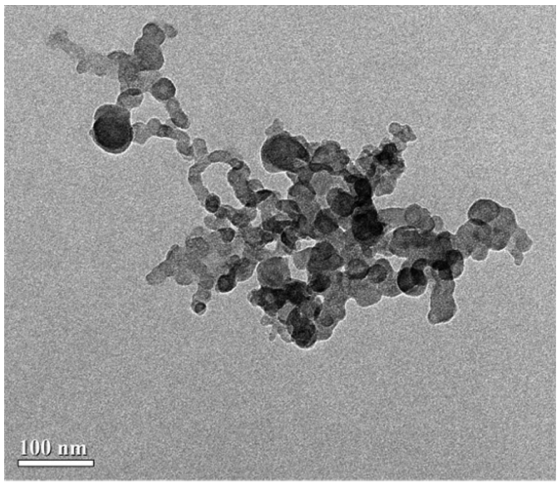


(a) Biodiesel engine's ultrafine particle

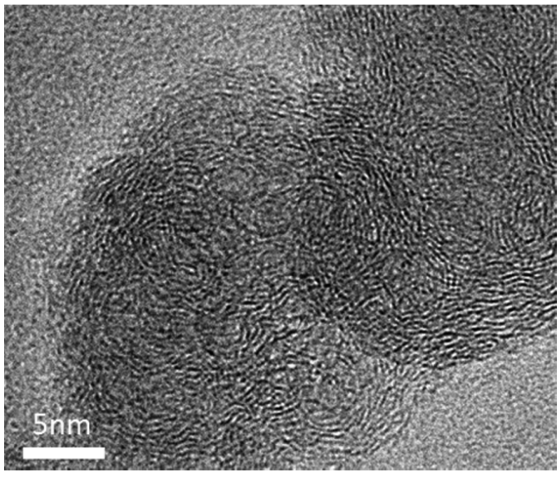


(b) Biodiesel engine's nanoparticle

Figure 5. TEM images of biodiesel engine's (a) Ultrafine particles and (b) Nanoparticles in the operation condition 80 % of engine load and 2,400 rpm of engine speed.

in the condition 80 % of engine load and 2,400 rpm of engine speed. The agglomerate ultrafine particle and primary nanoparticle size were micron and submicron scale, respectively. Engine's agglomerate ultrafine particles consist of several uniform primary nanoparticles. Most of engine's primary nanoparticle diameter is smaller than 60 nm. The average agglomerate ultrafine particle sizes of both diesel and biodiesel engine's PMs are approximately 100 nm ~ 500 nm. Figures 6 and 7 show TEM images of biodiesel and diesel engine's ultrafine PMs under the condition 80 % of engine load, 2,400 rpm of engine speed and carbon black ultrafine particles. The average agglomerated ultrafine particle's diameter of carbon black is significant larger than that of diesel and biodiesel engine PMs. Primary nanoparticles of both diesel and biodiesel engine's PMs were measured using image processing method.

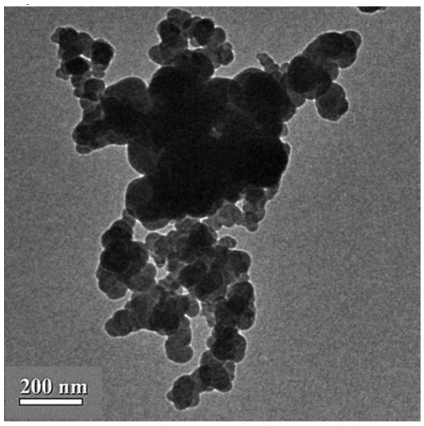


(a) Carbon black ultrafine particle

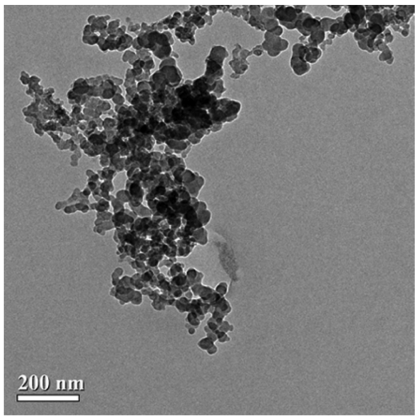


(b) Diesel engine's ultrafine particle

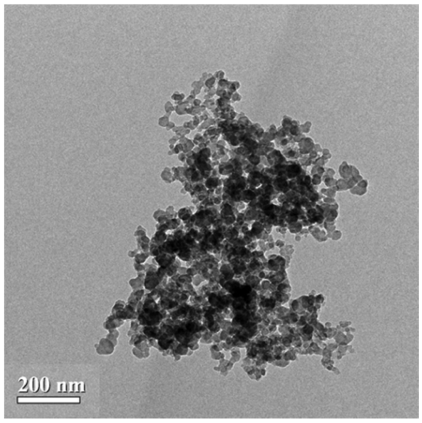


(c) Biodiesel engine's ultrafine particle

Figure 6. TEM images of (a) Carbon black; (b) Diesel engine's ultrafine particles; (c) Biodiesel engine's ultrafine particles in the operation condition 80 % of engine load and 2,400 rpm of engine speed.

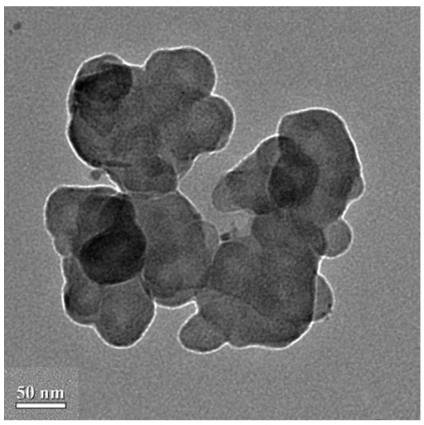


(a) Carbon black ultrafine particle

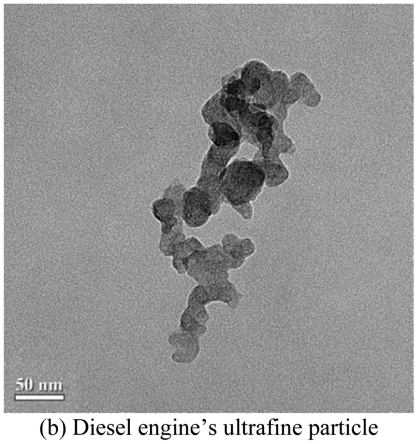


(b) Diesel engine's ultrafine particle

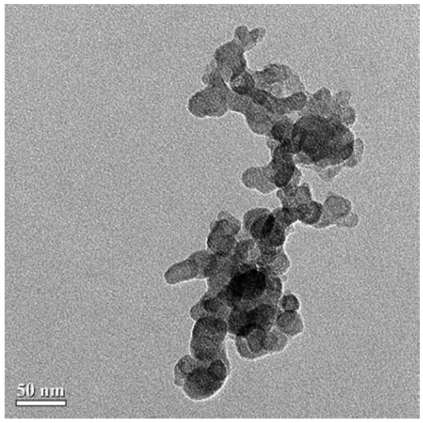


(c) Biodiesel engine's ultrafine particle

Figure 7. TEM images of (a) Carbon black; (b) Diesel engine's ultrafine particles; (c) Biodiesel engine's ultrafine particles in the operation condition 80 % of engine load and 2,400 rpm of engine speed.

One hundred primary nanoparticles of each case are successfully measured using the image processing software. Figures 8 and 9 show biodiesel and diesel engine's primary nanoparticle size distribution in the condition 20, 40, 60 and 80 % of engine load and (a) 1,600, (b) 2,000 and (c) 2,400 rpm of engine speed, respectively. The primary nanoparticle diameters are in the range of 10 nm ~ 60 nm. It was clearly observed much amount of particle diameters are in the range of 30 nm ~ 40 nm.

Figure 10 shows the average diameter size of diesel engine's nanoparticles versus biodiesel engine's nanoparticles in 20, 40, 60 and 80 % of engine load and

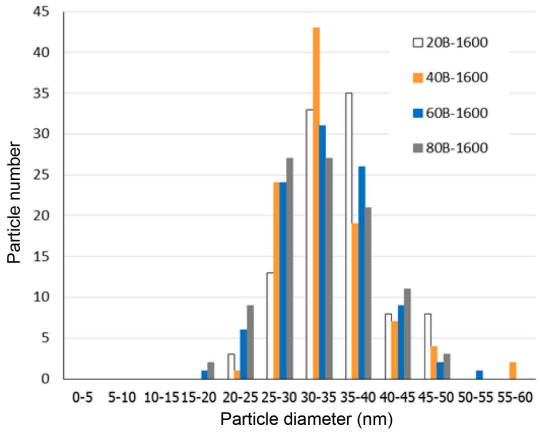


(a) Biodiesel engine 1600 rpm

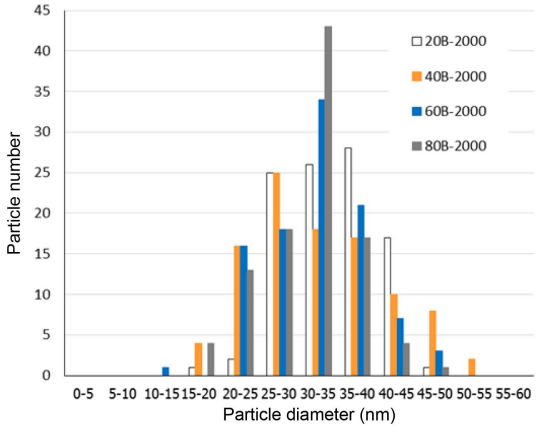


(b) Biodiesel engine 2000 rpm

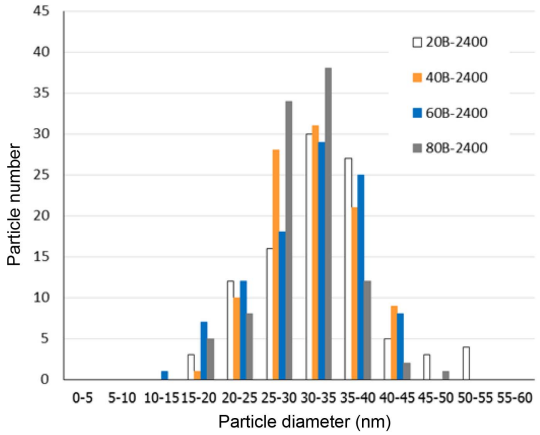


(c) Biodiesel engine 2400 rpm

Figure 8. Size distributions of biodiesel engine's nanoparticle emissions using TEM image processing method. The engine operation conditions are 20, 40, 60 and 80 % of engine load and (a) 1,600; (b) 2,000; (c) 2,400 rpm of engine speed, respectively.

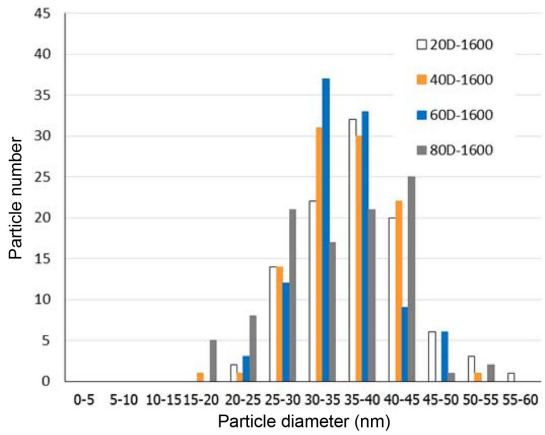


(a) Diesel engine 1600 rpm

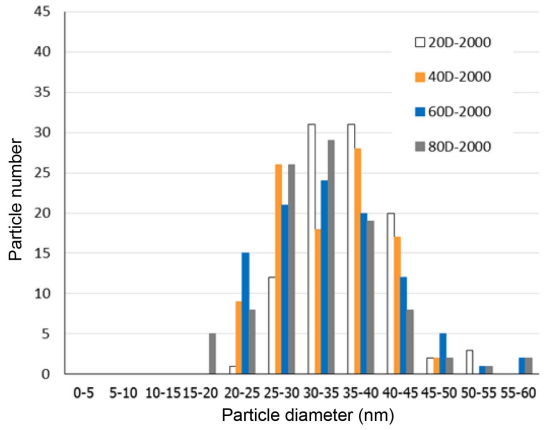


(b) Diesel engine 2000 rpm

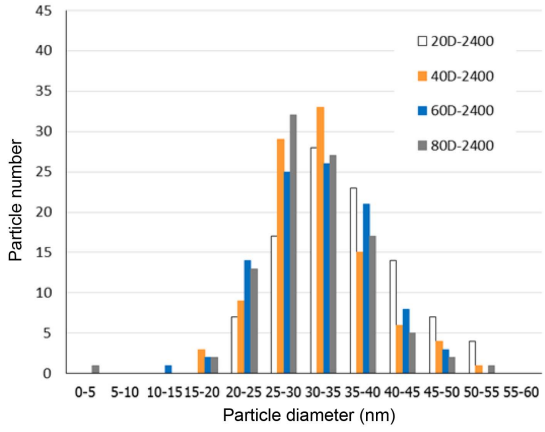


(c) Diesel engine 2400 rpm

Figure 9. Size distributions of diesel engine's nanoparticle emissions using TEM image processing method. The engine operation conditions are 20, 40, 60 and 80 % of engine load and (a) 1,600; (b) 2,000; (c) 2,400 rpm of engine speed, respectively.

1,600, 2,000 and 2,400 rpm of engine speed. Particle diameter size decreased when increasing engine speed for both of diesel and biodiesel's engine PMs. The exhaust gas temperature also gradually increased when increasing engine speed. It means PM oxidation rate inside combustion chamber increased when increasing engine

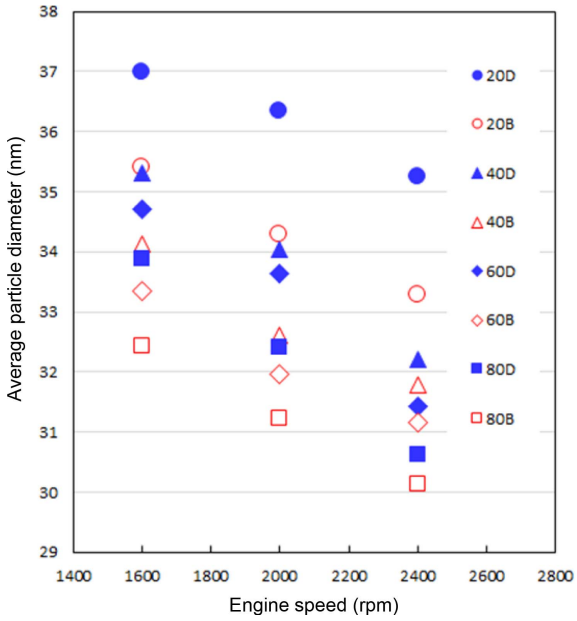


Figure 10. Average particle size of diesel engine's nanoparticles versus biodiesel engine's nanoparticles under 20, 40, 60 and 80 % of engine load and 1,600, 2,000 and 2,400 rpm of engine speed using TEM image processing method.

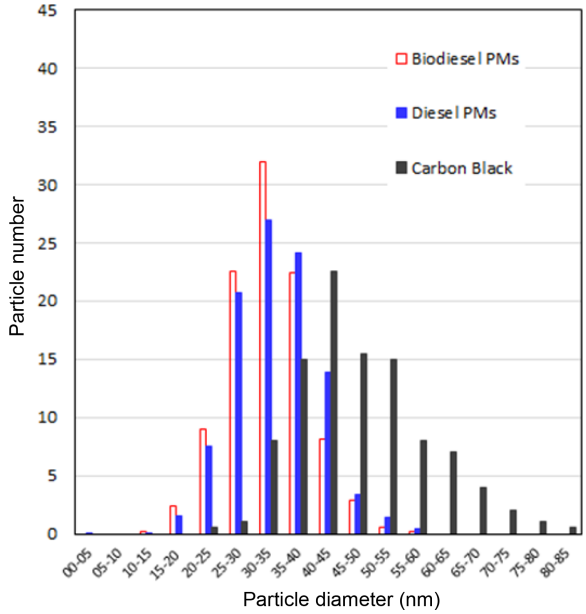


Figure 11. Size distribution of carbon black versus average particle size distribution of diesel engine's nanoparticles and biodiesel engine's nanoparticles under 20, 40, 60 and 80 % of engine load and 1,600, 2,000 and 2,400 rpm of engine speed using TEM image processing method.

speed (increasing temperature) due to lower heat loss on cylinder surface compare to lower engine speed. Similarly, particle diameter size decreased when increasing engine load for both of diesel and biodiesel's engine PMs. The exhaust gas temperature also gradually increased when increasing the engine load. It means PM oxidation rate inside combustion chamber increased when increasing engine load (increasing fuel injection quantity) resulting in higher combustion temperature compare to lower engine load. Moreover, the average diameter of biodiesel engine's PMs are significantly smaller than that of diesel engine's PMs because of bio-oxygenate fule. The average diameter of primary nanoparticles emitted from engine all operation conditions and carbon black are in the range of 10 nm ~ 60 nm and 20 nm ~ 90 nm, respectively, as shown in Figure 11. The average single particle sizes of carbon black, diesel and biodiesel engine's PMs are approximately 48, 34 and 32 nm, respectively.

### 3.2. Particulate Matters Oxidation Kinetics

Figures 12 show mass conversions of carbon black, diesel engine's PMs and biodiesel engine's PMs oxidation with pure air on DPF powders using TGA isothermal method in the condition of (a) 500, (b) 550 and (c) 600 °C, respectively. It was clearly seen that biodiesel engine's PMs were oxidized faster than diesel engine's PMs. Engine's PMs could be oxidized fastest in the condition of 600 °C and slowest in the condition of 500 °C for both of carbon black and engine's PMs. Absolutely, engine's PMs oxidation rate is higher than carbon black. Figure 13 shows Arrhenius plots of PMs oxidation rate on DPF powders. PMs oxidation rate of 20 % ~ 40 %, 40 % ~ 60 %, 60 % ~ 80 % burned fraction of all cases were clearly observed. The slope of carbon black is higher than that of engine's PMs. Table 3 shows the Apparent activation energies of engine's PMs oxidation on conventional cordierite DPF powders with pure air are in the range of 109 ~ 131 kJ/mole. The lowest apparent activation energies of biodiesel and diesel engine's PMs oxidation on conventional cordierite DPF powders are 109 and 117 kJ/mole, respectively. This lowest apparent activation energy occurred in 20 % ~ 40 % of mass burned fraction. Whereas, the highest apparent activation energies of 60 % ~ 80 % of biodiesel and diesel engine's PMs mass burned fraction on DPF powders are 131 and 130 kJ/mole, respectively. It was clearly observed that apparent activation energy of pure PMs oxidation are higher (Karin *et al*., 2015) than that of PMS oxidiation on DPF powder.

## 4. CONCLUSION

Quantity, morphology and oxidation kinetics of biodiesel engine's PMs were characterized successfully. The quantities of PMs emitted from biodiesel engine are approximately a half of diesel engine's PMs. Average primary nanoparticle sizes of carbon black particles, diesel and biodiesel engine's PMs are approximately 48, 34 and 32 nm, respectively. The quantity and primary particle size

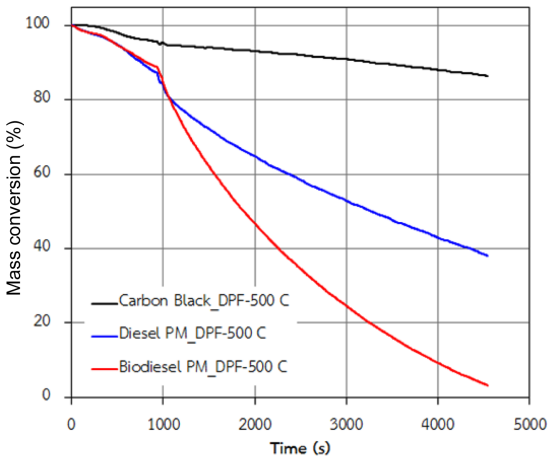


(a) Pure air isothermal 500 ºC

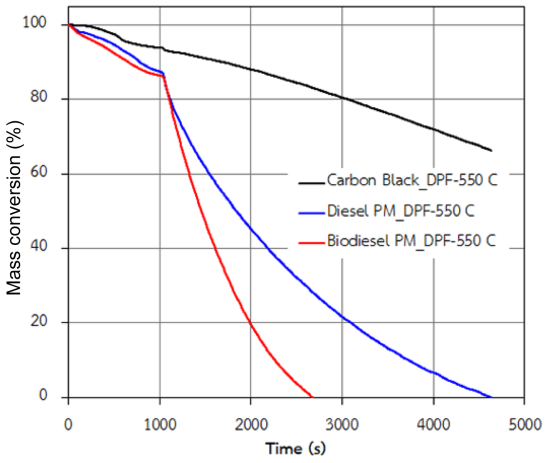


(b) Pure air isothermal 550 ºC

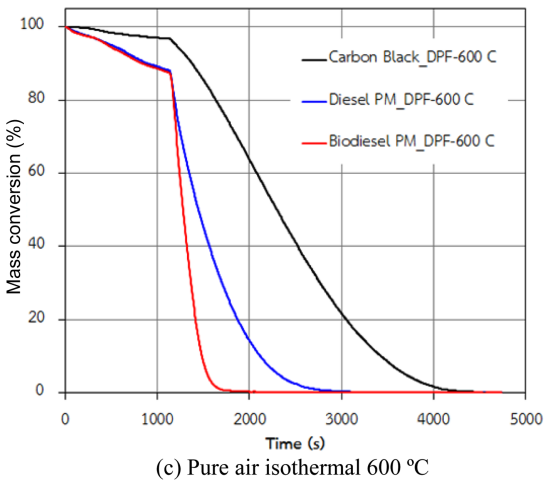


(c) Pure air isothermal 600 ºC

Figure 12. Oxidation kinetics of carbon black, diesel engine's PMs and biodiesel engine's PMs on conventional cordierite DPF powders using TGA isothermal method: (a) 500 ºC; (b) 550 ºC; (c) 600 ºC with pure air.

of engine's PMs decreased when increasing the engine speed and engine load because of combustion temperature

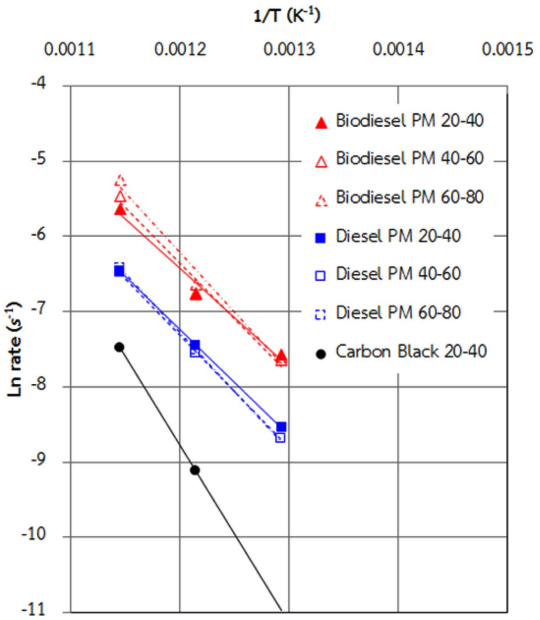


Figure 13. Arrhenius plots of carbon black, diesel engine's PMs and biodiesel engine's PMs oxidation on conventional cordierite DPF powders using TGA isothermal method, 500-550-600 ºC with pure air.

Table 3. Calculated apparent activation energies (*Ea*) of engine's PMs oxidize on conventional cordierite DPF powder with pure air.

| | Apparent activation energy *Ea* (kJ/mole) |
|---|---|
| PMs oxidize with DPF powder | |
| PMs burned fraction | |
| Biodiesel engine's PMs | 121 ± 11 |
| Biodiesel 20 % ~ 40 % burned | 109 |
| Biodiesel 40 % ~ 60 % burned | 121 |
| Biodiesel 60 % ~ 80 % burned | 131 |
| Diesel engine's PMs | 124 ± 7 |
| Diesel 20 % ~ 40 % burned | 117 |
| Diesel 40 % ~ 60 % burned | 124 |
| Diesel 60 % ~ 80 % burned | 130 |
| Pure PMs oxidize without DPF powder | |
| Biodiesel engine's PMs | 152 ± 5 (Karin *et al.*, 2015) |
| Diesel engine's PMs | 159 ± 6 (Karin *et al.*, 2015) |

is also automatically increased.

Engine's PMs are easier to oxidize than carbon black nanoparticles because of unburned hydrocarbon and also smaller size of particle. The oxidation rate of biodiesel

engine's PMs are higher than that of diesel engine PMs because of unburned bio-oxygenate hydrocarbon and smaller size of particle. Calculated apparent activation energies of biodiesel engine's PM oxidation on conventional cordierite DPF powder are lower than that of diesel engine's PM and carbon black nanoparticles. The apparent activation energies of biodiesel engine's PM and diesel engine's PM oxidation on conventional cordierite DPF powders are 121 ± 11 kJ/mole and 124 ± 7 kJ/mole, respectively.

Oxygen atom included inside oxygenated fuel molecules might promote lower PM oxidation activation energy. However, oxidation rate of particulate matters is strongly related to not only apparent activation energy but also physical impact, such as primary particle size which are strongly related to the reaction order and frequency factor. Smaller primary nanoparticle diameter of biodiesel engine would be an advantage of DPF regeneration process in vehicle application.

**ACKNOWLEDGEMENT**–The authors gratefully acknowledge the financial support from Thailand Research Fund (TRF), Thailand.

## REFERENCES

Choi, S., Myung, C. L. and Park, S. (2014). Review on characterization of nano-particle emissions and morphology from internal combustion engines: Part 2. *Int. J. Automotive Technology* **15**, **2**, 219–227.

Choi, S. and Seong, H. (2015). Oxidation characteristics of gasoline direct-injection (GDI) engine soot: Catalytic effects of ash and modified kinetics correlation. *Combustion and Flame* **162**, **6**, 2371–2389.

Darcy, P., Costa, P. D., Mellottee, H., Trichard, J. M. and Mariadassou, G. D. (2007). Kinetics of catalyzed and non-catalyzed oxidation of soot from a diesel engine. *Catalysis Today* **119**, **1-4**, 252–256.

Eastwood, P. (2008). *Particulate Emissions from Vehicles*. SAE International and John Wiley & Sons, Ltd. Pennsylvania, USA.

Fino, D. and Specchai, V. (2008). Review open issues in oxidative catalysis for diesel particulate abatement. *Powder Technology*, **180**, 64–73.

Hanamura, K., Karin, P., Cui, L., Rubio, P., Tsuruta, T., Tanaka, T. and Suzuki, T. (2009). Micro- and macroscopic visualization of particulate matter trapping and regeneration processes in wall-flow diesel particulate filters. *Int. J. Engine Research*, **10**, 305–321.

Ishiguro, T., Takatori, Y. and Akihama, K. (1997). Cutler W. A. and Warren, C. J. (2001). Microstructure of diesel soot particles probed by electron microscopy: First observation of inner core and outer shell. *Combustion and Flame* **108**, **1**, 231–234.

Karin, P., Cui, L., Rubio, P., Tsuruta, T. and Hanamura, K. (2009). Microscopic visualization of PM trapping and regeneration in micro-structural pores of a DPF wall. *SAE Int. J. Fuels and Lubricants* **2**, **1**, 661–669.

Karin, P. and Hanamura, K. (2010). Particulate matter trapping and oxidation on catalyst-membrane. *SAE Int. J. Fuels and Lubricants* **3**, **1**, 368–379.

Karin, P., Songsaengchan, Y., Laosuwan, S., Charoenphonphanich, C., Chollacoop, N. and Hanamura, K. (2013a). Nanostructure investigation of particle emission by using TEM image processing method. *Energy Procedia*, **34**, 757–766.

Karin, P., Songsaengchan, Y., Laosuwan, S., Charoenphonphanich, C., Chollacoop, N. and Hanamura, K. (2013b). Physical characterization of biodiesel particle emission by electron microscopy. *SAE Paper No*. 2013-32-9150.

Karin, P., Borhanipour, M., Songsaengchan, Y., Laosuwan, S., Charoenphonphanich, C., Chollacoop, N. and Hanamura, K. (2015). Oxidation kinetics of small CI engine's biodiesel particulate matter. *Int. J. Automotive Technology* **16**, **2**, 211–219.

Kittelson, D. B. (1998). Engines and nanoparticles: A review. *J. Aerosol Science* **29**, **5-6**, 575–588.

Lee, K. O., Seong, H. and Choi, S. M. (2013a). Detailed analysis of kinetic reactions in soot oxidation by simulated diesel exhaust emissions. *Proc. Combustion Institute* **34**, **2**, 3057–3065.

Lee, S., Lee, D. and Choi, S. C. (2013b). Impact of SME blended fuel combustion on soot morphological characteristics in a diesel engine. *Int. J. Automotive Technology* **14**, **5**, 757–762.

Maricq, M. M. (2007). Review chemical characterization of particulate emissions from diesel engine: A review. *J. Aerosol Science* **38**, **11**, 1079–1118.

Myung, C. L., Ko, A. and Park, S. (2014). Review on characterization of nano-particle emissions and PM morphology from internal combustion engines: Part 1. *Int. J. Automotive Technology* **15**, **2**, 203–218.

Neeft, J. A., Makkee, M. and Moulijn, J. (1996). Diesel particulate emission control. *Fuel Processing Technology* **47**, **1**, 1–69.

Neeft, J. A., Nijhuis, T. X., Smakman, E., Makkee, M. and Moulijn, J. A. (1997). Kinetics of the oxidation of diesel soot. *Fuel* **76**, **12**, 1129–1136.

Oki, H., Karin, P. and Hanamura, K. (2011). Visualization of oxidation of soot nanoparticles trapped on a diesel particulate membrane filter. *SAE Int. J. Engines* **4**, **1**, 515–526.

Smith, O. I. (1981). Fundamentals of soot formation in flames with application to diesel engine particulate emissions. *Prog. Energy and Combustion Science* **7**, **4**, 275–291.

Soylu, S. (2014). Examination of PN emissions and size distributions of a hybrid city bus under real world urban driving conditions. *Int. J. Automotive Technology* **15**, **3**, 369–376.

Vander Wal, R. L., Yezerets, A., Currier, N. W., Kim, D. H.

and Wang, C. H. (2007). HRTEM study of diesel soot collected from diesel particulate filters. *Carbon* **45**, **1**, 70–77.

Yezerets, A., Currier, N. W., Kin, D. H., Eadler, H. A., Epling, W. S. and Peden, C. H. F. (2005). Differential kinetic analysis of diesel particulate matter (soot) oxidation by oxygen using a step-response technique. *Applied Catalysis B: Environmental* **61**, **1-2**, 120–129.

IJAT International Journal of Automotive Technology KSAE

Jul. 16. 2016

## [IJAT] Paper No. 220160025

### ■ Certificate of PrePublication ■

The Editorial Board of the IJAT hereby certifies that the following paper is scheduled to be published in the IJAT(Volume 0 , Number 0, 0).

| | |
|---|---|
| Paper No. | 220160025 |
| Paper Title | MORPHOLOGY AND OXIDATION KINETICS OF CI ENGINE'S BIODIESEL PARTICULATE MATTERS ON CORDIERITE DIESEL PARTICULATE FILTERS USING TGA |
| Category | Engine, Emission Technology |
| Author(s) | Dr. Preechar Karin (King Mongkut's Institute of Technology Ladkrabang)*, Dr. J. BOONSAKDA (King Mongkut's Institute of Technology Ladkrabang, Bangkok), Dr. K. SIRICHOLATHUM (King Mongkut's Institute of Technology Ladkrabang, Bangkok), Dr. E. SAENKHUMVONG (King Mongkut's Institute of Technology Ladkrabang), Dr. C. CHAROENPHONPHANICH (King Mongkut's Institute of Technology Ladkrabang), Dr. K. HANAMURA (Tokyo Institute of Technology) |

The Korean Society of Automotive Engineers
Editor-in-Chief
Int. J. Automotive Technology

- IJAT Web Site : http://www.ijat.net

13th Fl. Paradise Venture Tower, 21 52-gil Teheran-ro, Gangnam-gu, Seoul 06212 , Korea
TEL +82-2-564-3971/2 FAX +82-2-564-3973 E-mail car@ksae.org

IJAT International Journal of Automotive Technology KSAE

Jul. 15. 2016

## [IJAT] Paper No. 220160025

## ■ Certificate of Acceptance ■

The Editorial Board of the IJAT hereby certifies that the following paper has been accepted for publication in the IJAT.

| | |
|---|---|
| Paper No. | 220160025 |
| Paper Title | MORPHOLOGY AND OXIDATION KINETICS OF CI ENGINE'S BIODIESEL PARTICULATE MATTERS ON CORDIERITE DIESEL PARTICULATE FILTERS USING TGA |
| Category | Engine, Emission Technology |
| Author(s) | Dr. Preechar Karin (King Mongkut's Institute of Technology Ladkrabang)*, Dr. J. BOONSAKDA (King Mongkut's Institute of Technology Ladkrabang, Bangkok), Dr. K. SIRICHOLATHUM (King Mongkut's Institute of Technology Ladkrabang, Bangkok), Dr. E. SAENKHUMVONG (King Mongkut's Institute of Technology Ladkrabang), Dr. C. CHAROENPHONPHANICH (King Mongkut's Institute of Technology Ladkrabang), Dr. K. HANAMURA (Tokyo Institute of Technology) |
| Review Result | Accept without further modification |

The Korean Society of Automotive Engineers
Editor-in-Chief
Int. J. Automotive Technology

- IJAT Web Site : http://www.ijat.net

13th Fl. Paradise Venture Tower, 21 52-gil Teheran-ro, Gangnam-gu, Seoul 06212 , Korea
TEL +82-2-564-3971/2 FAX +82-2-564-3973 E-mail car@ksae.org